Earthquakes and Structures, *Vol. 17, No. 2 (2019) 143-162*
DOI: https://doi.org/10.12989/eas.2019.17.2.143

Active tuned tandem mass dampers for seismic structures

Chunxiang Li* and Liyuan Cao

Department of Civil Engineering, Shanghai University, No. 99 Shangda Road, Shanghai 200444, P. R. China

(Received March 27, 2019, Revised April 29, 2019, Accepted May 5, 2019)

Abstract. Motivated by a simpler and more compact hybrid active tuned mass damper (ATMD) system with wide frequency spacing (i.e., high robustness) but not reducing the effectiveness using the least number of ATMD units, the active tuned tandem mass dampers (ATTMD) have been proposed to attenuate undesirable oscillations of structures under the ground acceleration. Likewise, it is expected that the frequency spacing of the ATTMD is comparable to that of the active multiple tuned mass dampers (AMTMD) or the multiple tuned mass dampers (MTMD). In accordance with the mode generalised system in the specific vibration mode being controlled (simply referred herein to as the structure), the closed-form expression of the dimensionless displacement variances has been derived for the structure with the attached ATTMD. The criterion for the optimum searching may then be determined as minimization of the dimensionless displacement variances. Employing the gradient-based optimization technique, the effects of varying key parameters on the performance of the ATTMD have been scrutinized in order to probe into its superiority. Meanwhile, for the purpose of a systematic comparison, the optimum results of two active tuned mass dampers (two ATMDs), two tuned mass dampers (two TMDs) without the linking damper, and the TTMD are included into consideration. Subsequent to work in the frequency domain, a real-time Simulink implementation of dynamic analysis of the structure with the ATTMD under earthquakes is carried out to verify the findings of effectiveness and stroke in the frequency domain. Results clearly show that the findings in the time domain support the ones in the frequency domain. The whole work demonstrates that ATTMD outperforms two ATMDs, two TMDs, and TTMD. Thereinto, a wide frequency spacing feature of the ATTMD is its highlight, thus deeming it a high robustness control device. Furthermore, the ATTMD system only needs the linking dashpot, thus embodying its simplicity.

Keywords: structural vibration control; active tuned tandem mass dampers; closed-form dimensionless displacement variances; frequency spacing; optimization; ground acceleration

1. Introduction

There are passive, semi-active, and active control devices for vibration mitigation of civil engineering structures in general (Spencer and Nagarajaiah 2003). Among these vibration control devices, a simple passive control device is the tuned mass damper (TMD), widely used worldwide. The TMD is a dynamic vibration absorber (DVA), composing of a single-degree-of-freedom (SDOF) mass block, attached to the primary structure through a spring and a viscous damper. Firstly, the spring stiffness is tuned to absorb the input energy from external disturbances effectively and simultaneously the structural vibration energy is transferred to the TMD. Then, the transferred energy is dissipated via the damping force introduced through the inertia force of a SDOF mass block, thereby achieving the target of the structural dynamic response reduction. The TMD is tuned near the target resonance frequency of the mode generalised system in the specific vibration mode being controlled (simply referred herein to as the structure, in practical terms, the SDOF structure), hence damping only one mode of the vibration. Because of its simple and reliable implementation, the applications of the TMD for civil engineering structures have been investigated and extended by, for example, Chung *et al.* Chung *et al.* (2013), Lu and Chen (2011, 2011), Lu *et al.* (2017), Gu *et al.* (1994), Casalotti *et al.* (2014), Carpineto *et al.* (2014), Domaneschi *et al.* (2015), Shu *et al.* (2017), Zhang *et al.* (2013), Si *et al.* (2014), Stewart and Lackner (2014), Li *et al.* (2015), Kaiming and Hong (2016), Song *et al.* (2016), Matta (2013), Lavan (2017), Kaveh *et al.* (2015), and Leung and Zhang (2009).

Notwithstanding the bright prospect of the TMD, on the inherent characteristics, the TMD is capable of enhancing performances of the protected structures under the narrow band excitations, such as wind loads, traffic loads, sea waves, as well as earthquakes with limited band frequency. Evidently, the band of tuning frequency (called the band of suppression frequency) in which the structural vibration can be suppressed by a TMD is very narrow. It goes without saying that the high sensitivity to tuning poses a serious concern of the TMD. Due to mistuned frequency, the vibration suppression performance of the TMD will be impaired significantly, in practical terms, meaning that the TMD is not all robust. The robustness of the TMD effectively refers to its ability against the change or estimation error in the structural natural frequency.

On the other hand, for practical reasons, the auxiliary mass (i.e., TMD mass block) is limited to on the order of several percent of total mass of the structure. This

*Corresponding author, Ph.D.
E-mail: Li-chunxiang@vip.sina.com

ISSN: 2092-7614 (Print), 2092-7622 (Online)

restriction makes the TMD less effective for strong earthquakes. The mass ratio effect of the TMD was investigated by carrying out numerical analyses under different earthquake records for SDOF structures with lots of periods (Bekdaş and Nigdeli 2013). A general observation is that the mass ratio of the TMD needs to be much higher (beyond 5%) for a higher performance of structures in the near-field ground motions (Li and Cao 2015). Therefore, it is necessary to research and develop the TMD devices endowed with large mass ratio. Delightedly, Angelis *et al.* (2012), Reggio and Angelis (2015) have recently explored the non-conventional tuned mass damper (TMD) with large mass ratio for mitigating the seismic risk of both new and existing buildings. For tall buildings, however, the mass ratio of the TMD must be kept in minimum levels. Hence, when needing to enhance the performance of earthquake-resistant structures by resorting to the TMD, we need to deal with its detuning effect and demand on large mass ratio.

In an attempt to remedy the detuning effect of the TMD, more than one tuned mass damper with different dynamic characteristics, that is the double and multiple tuned mass dampers (DTMD and MTMD) have been proposed and investigated by, for example, Li and Zhu (2006), Ok *et al.* (2009), Xu and Igusa (1992), Kareem and Kline (1995), Jangid (1995, 1999), Li (2000), Li and Liu (2003), Li and Qu (2006), Li and Liu (2002), Zuo and Nayfeh (2005), Lin *et al.* (2010, 2010), Fu and Johnson (2011), Jokic *et al.* (2011), Daniel *et al.* (2012), Stăncioiu and Ouyang (2012), Mohebbi *et al.* (2013), Dinh and Basu (2015). Likewise, the semi-active tuned mass damper (SATMD) with minimal power is also thought of as a promising solution to the detuning problem of the TMD, because of its unique feature in real-time updating the stiffness or damping of the TMD making use of the sensed data on the actual vibration states of the structures, for example, Nagarajaiah and Varadarajan (2005), Nagarajaiah and Sonmez (2007), Nagarajaiah (2009), Weber *et al.* (2011), Chung *et al.* (2013), Sun and Nagarajaiah (2014), Weber (2014), Lin *et al.* (2015), Sun (2018), Chey (2010), Lin *et al*. (2012), Kaveh *et al.* (2015). But, it is worth mentioning that owing to online update, the semi-active tuned mass damper is more applicable to systems with time-variant parameters (Sun 2018). For example, the stiffness of the structures in elasto-plastic states (i.e., damage states) will be degenerating during severe earthquake events. Earthquakes could be highly non-stationary, thus meaning that the structural responses possess the time-variant energy and frequency content (Basu and Nagarajaiah 2008). Likewise, earthquakes can involve a broad range of frequencies. In these cases, The SATMD with adjustable dynamic parameters is adaptive to changes in the structural behaviour over time and provides a broad feedback adaptive range of control, thus reducing the structural responses.

As regards impulsive earthquake applications, the TMD may reduce the structural seismic responses when a large mass ratio is taken into consideration (Chen and Wu 2001). But, this heavier additional mass will need an extraordinarily large space and thus, its use becomes economically impractical. In practical terms, the original plan of installing the TMD for a project is often abandoned, since the stroke of the TMD is too large and there is not enough space to house it. But glad to notice that the effectiveness of the TMD may be further enhanced through introducing an active force to act between the controlled structure and the TMD, then comprising the active tuned mass damper (ATMD) (Chang and Soong 1980) Hence, a very promising alternative to surmount this large mass ratio restriction is to take advantage of the ATMD to achieve better attenuation in the structural displacement and/or acceleration against the impulsive earthquakes. Likewise, the research in optimizing the feedback gains and damper characteristics of an ATMD system in order to minimize the structural displacements and/or accelerations has nowadays been carried out by many researchers, for example, Chang and Yang (1995), Ankireddi and Yang (1996), Yan *et al.* (1999), Nagashima (2001), Nishitani and Inoue (2001), Collins *et al.* (2006), Guclu and Yazici (2008), Li *et al.* (2010), Venanzi *et al.* (2013), Amini *et al.* (2013), Fitzgerald and Basu (2014), and Li and Cao (2019). However, the robustness of the ATMD is not to be compared with that of the MTMD. Happily, the robustness of the ATMD can be remarkably enhanced using the active multiple tuned mass dampers (AMTMD) with decentralized control force feature (Li *et al.* 2002, 2003).

Despite these research progresses, it is imperative and of practical interest to further search for a simpler and more compact hybrid active tuned mass damper system with wide frequency spacing (i.e., high robustness against the change or estimation error in the structural natural frequencies) but not reducing the effectiveness using the least number of ATMD units. To this end, two active tuned mass dampers, with the least number, are taken into consideration to enhance the robustness of a single active tuned mass damper, and then creating a new control device. As far as the two active tuned mass dampers are concerned, there exist two ways of composition. Series of two active tuned mass dampers forms the hybrid active tuned mass dampers (HATMD) and the enhanced hybrid active tuned mass dampers (EHATMD) (Li and Cao 2015, Cao and Li 2018). The parallel connection of two tuned mass dampers with a linking dashpot between mass blocks to structure constitutes the tuned tandem mass dampers (TTMD) (Yang and Li 2017) and Tuned tandem mass dampers-inerters (TTMDI) (Cao and Li 2019). Along these lines, the present paper further proposes a novel device, named the active tuned tandem mass dampers (ATTMD), which are anticipated to have high robustness. Therefore, the first work of the present study is to present the closed-form expression in the frequency domain and investigate the performance of the ATTMD by extensive simulation results based on the selected criteria for the optimality under the ground acceleration. Subsequent to the first work, a real-time Simulink implementation of dynamic analysis of the structure with the ATTMD, including comparison object: two ATMDs without the linking dashpot under actual and artificial earthquake records is carried out to verify the findings of effectiveness and stroke in the frequency domain.

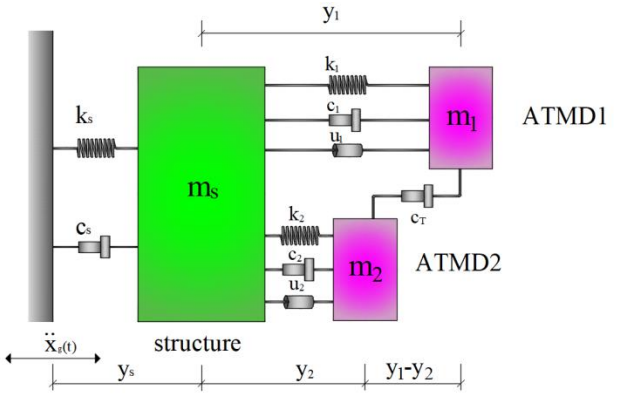

Fig. 1 Mechanical model of the active tuned tandem mass dampers (ATTMD) system

2. Closed-form expressions for dimensionless displacement variances of the ATTMD structure system

Fig. 1 presents the mechanical model of the active tuned tandem mass dampers (ATTMD) located on a single-degree-of-freedom (SDOF) structure, as previously mentioned, effectively representing the mode generalised system in the specific vibration mode being controlled of the multi-degrees-of-freedom (MDOF) structures, excited by the ground acceleration [$\ddot{x}_g(t)$]. The present control system configuration contains both the ATMD1 and ATMD2. Likewise, a linking dashpot is introduced between the ATMD1 and ATMD2. The set of second-order differential equations of motion for the structure ATTMD system can then be established as follows

$$m_s\left[\ddot{x}_g(t)+\ddot{y}_s\right]+c_s\dot{y}_s+k_s y_s-c_1\dot{y}_1-k_1y_1-c_2\dot{y}_2-k_2y_2 = -u_1(t)-u_2(t) \tag{1}$$

$$m_1\left[\ddot{x}_g(t)+\ddot{y}_s+\ddot{y}_1\right]+c_1\dot{y}_1+k_1y_1+c_T\left(\dot{y}_1-\dot{y}_2\right)=u_1(t) \tag{2}$$

$$m_2\left[\ddot{x}_g(t)+\ddot{y}_s+\ddot{y}_2\right]+c_2\dot{y}_2+k_2y_2-c_T\left(\dot{y}_1-\dot{y}_2\right)=u_2(t) \tag{3}$$

in which m_s, m_1, and m_2 are the mass of the structure, ATMD1, and ATMD2, respectively; c_s, c_1, and c_2 represent the viscous damping coefficients of the structure, ATMD1, and ATMD2, respectively; c_T stands for the linking viscous damping coefficient introduced between the ATMD1 and ATMD2; k_s, k_1, and k_2 refer to the stiffness coefficients of the structure, ATMD1, and ATMD2, respectively; y_s, y_1, and y_2 denote the relative displacements of the structure, ATMD1, and ATMD2 with reference to their respective supports, that are the ground and structure, respectively; and, $u_1(t)$ and $u_2(t)$ indicate the active control forces generated by the actuators in the ATMD1 and ATMD2, respectively, which are to be explicitly defined below.

Next, suppose that calculating active control forces of the ATTMD system in real time by resorting to feeding back the sensing signal can be written in a compact representation as follows

$$u_1(t)=-\bar{m}_1\ddot{y}_s-\bar{c}_1\dot{y}_1-\bar{k}_1y_1 \tag{4}$$

$$u_2(t)=-\bar{m}_2\ddot{y}_s-\bar{c}_2\dot{y}_2-\bar{k}_2y_2 \tag{5}$$

where $\bar{m}_1$ and $\bar{m}_2$, respectively, indicate the gains of both the ATMD1 and ATMD2, feeding back the acceleration of the structure; while $\bar{c}_1$ and $\bar{k}_1$, $\bar{c}_2$ and $\bar{k}_2$ correspond, respectively, to the gains of feeding back the velocity and displacement of the respective ATMDs, namely the ATMD1 and ATMD2.

In order to render a compact formulation, we beforehand introduce the following new variables.

$$\omega_s=\sqrt{\frac{k_s}{m_s}},\quad \omega_1=\sqrt{\frac{k_1+\bar{k}_1}{m_1}},\quad \omega_2=\sqrt{\frac{k_2+\bar{k}_2}{m_2}},\quad \omega_T=\frac{\omega_1+\omega_2}{2}$$

$$\xi_s=\frac{c_s}{2m_s\omega_s},\quad \xi_1=\frac{c_1+\bar{c}_1}{2m_1\omega_1},\ \xi_2=\frac{c_2+\bar{c}_2}{2m_2\omega_2},\quad \xi_T=\frac{c_T}{2(m_1+m_2)\omega_T}$$

$$\mu_1=\frac{m_1}{m_s},\quad \mu_2=\frac{m_2}{m_s},\quad \mu_T=\mu_1+\mu_2$$

$$\alpha_1=\frac{\bar{m}_1}{m_1},\quad \alpha_2=\frac{\bar{m}_2}{m_2},\quad \alpha_T=\alpha_1+\alpha_2$$

$$\eta=\frac{m_1}{m_2},\quad \gamma=\frac{\alpha_1}{\alpha_2}$$

Denote the Laplace transforms of the displacement, velocity, acceleration responses, and ground acceleration, respectively by

$$Y_s(s)=L[y_s(t)],\ Y_1(s)=L[y_1(t)],\ Y_2(s)=L[y_2(t)],$$
$$sY_s(s)=L[\dot{y}_s(t)],\ sY_1(s)=L[\dot{y}_1(t)],\ sY_2(s)=L[\dot{y}_2(t)],$$
$$s^2Y_s(s)=L[\ddot{y}_s(t)],\ s^2Y_1(s)=L[\ddot{y}_1(t)],\ s^2Y_2(s)=L[\ddot{y}_2(t)],$$
$$\ddot{X}_g(s)=L[\ddot{x}_g(t)]\cdot$$

Employing Eqs. (4) and (5), the forms in the Laplace domain of Eqs. (1)-(3) can then be written, respectively as

$$\begin{aligned}&\ddot{X}_g(s)+\left[\left(1-\alpha_1\mu_1-\alpha_2\mu_2\right)s^2+2\xi_s\omega_s s+\omega_s{}^2\right]Y_s(s)\\&-\left(2\xi_1\mu_1\omega_1 s+\mu_1\omega_1{}^2\right)Y_1(s)\ -\left(2\xi_2\mu_2\omega_2 s+\mu_2\omega_2{}^2\right)Y_2(s)=0\end{aligned} \tag{6}$$

$$\begin{aligned}&\ddot{X}_g(s)+\left(1+\alpha_1\right)s^2Y_s(s)\\&+\left\{s^2+\left[2\xi_1\omega_1+\xi_T\frac{1+\eta}{\eta}\left(\omega_1+\omega_2\right)\right]s+\omega_1{}^2\right\}Y_1(s)\\&+\left[-\xi_T\frac{1+\eta}{\eta}\left(\omega_1+\omega_2\right)s\right]Y_2(s)=0\end{aligned} \tag{7}$$

$$\begin{aligned}&\ddot{X}_g(s)+\left(1+\alpha_2\right)s^2Y_s(s)+\left[-\xi_T\left(1+\eta\right)\left(\omega_1+\omega_2\right)s\right]Y_1(s)\\&+\left\{s^2+\left[2\xi_2\omega_2+\xi_T\left(1+\eta\right)\left(\omega_1+\omega_2\right)\right]s+\omega_2{}^2\right\}Y_2(s)=0\end{aligned} \tag{8}$$

Substituting $s=i\omega$ into Eqs. (6)-(8), where $\mathrm{i}=\sqrt{-1}$, and introducing non-dimensional coefficients: $\lambda=\frac{\omega}{\omega_s}$, $f_1=\frac{\omega_1}{\omega_s}$, $f_2=\frac{\omega_2}{\omega_s}$, Eqs. (6)-(8) can then be rewritten, respectively as the following forms

$$\begin{aligned}&\ddot{X}_g(\mathrm{i}\omega)/\omega_s^2+\left[C_{12}(\mathrm{i}\lambda)^2+C_{11}(\mathrm{i}\lambda)+C_{10}\right]Y_s(\mathrm{i}\omega)\\&+\left[D_{12}(\mathrm{i}\lambda)^2+D_{11}(\mathrm{i}\lambda)+D_{10}\right]Y_1(\mathrm{i}\omega)\\&+\left[E_{12}(\mathrm{i}\lambda)^2+E_{11}(\mathrm{i}\lambda)+E_{10}\right]Y_2(\mathrm{i}\omega)=0\end{aligned} \tag{9}$$

$$\begin{aligned}&\ddot{X}_g(\mathrm{i}\omega)/\omega_s^2+\left[C_{22}(\mathrm{i}\lambda)^2+C_{21}(\mathrm{i}\lambda)+C_{20}\right]Y_s(\mathrm{i}\omega)\\&+\left[D_{22}(\mathrm{i}\lambda)^2+D_{21}(\mathrm{i}\lambda)+D_{20}\right]Y_1(\mathrm{i}\omega)\\&+\left[E_{22}(\mathrm{i}\lambda)^2+E_{21}(\mathrm{i}\lambda)+E_{20}\right]Y_2(\mathrm{i}\omega)=0\end{aligned} \tag{10}$$

$$\ddot{X}_g(\mathrm{i}\omega)/\omega_s^2+\left[C_{32}(\mathrm{i}\lambda)^2+C_{31}(\mathrm{i}\lambda)+C_{30}\right]Y_s(\mathrm{i}\omega)+\left[D_{32}(\mathrm{i}\lambda)^2+D_{31}(\mathrm{i}\lambda)+D_{30}\right]Y_1(\mathrm{i}\omega)+\left[E_{32}(\mathrm{i}\lambda)^2+E_{31}(\mathrm{i}\lambda)+E_{30}\right]Y_2(\mathrm{i}\omega)=0 \tag{11}$$

For the sake of conciseness and compactness, the corresponding coefficients of Eqs. (9)-(11) are provided in Table 1.

Through simultaneously solving Eqs. (9)-(11), the transfer functions of the structure with the attached ATTMD, ATMD1, and ATMD2 can then be expressed in a compact form, respectively as below

$$G_s(\mathrm{i}\omega)=\frac{Y_s(\mathrm{i}\omega)}{\ddot{X}_g(\mathrm{i}\omega)}=\sum_{r=0}^{4}B_{sr}(\mathrm{i}\lambda)^r\Big/\omega_s^2\sum_{p=0}^{6}A_{sp}(\mathrm{i}\lambda)^p \tag{12}$$

$$G_1(\mathrm{i}\omega)=\frac{Y_1(\mathrm{i}\omega)}{\ddot{X}_g(\mathrm{i}\omega)}=\sum_{l=0}^{8}B_{Tl}(\mathrm{i}\lambda)^l\Big/\omega_s^2\sum_{q=0}^{10}A_q(\mathrm{i}\lambda)^q \tag{13}$$

$$G_2(\mathrm{i}\omega)=\frac{Y_2(\mathrm{i}\omega)}{\ddot{X}_g(\mathrm{i}\omega)}=\sum_{z=0}^{8}B_{tz}(\mathrm{i}\lambda)^z\Big/\omega_s^2\sum_{q=0}^{10}A_q(\mathrm{i}\lambda)^q \tag{14}$$

where

$$B_{sr}=\begin{cases}\vec{I}\bullet\overline{DE}_r, & r=0,1,...,4\\ 0, & r<0\end{cases},\quad A_{sp}=\begin{cases}\sum_{j=p-4}^{2}\vec{c}_j\bullet\overline{DE}_{p-j}, & p=0,1,...,6\\ 0, & p<0\end{cases}$$

$$B_{Tl}=\sum_{i=I-6}^{2}(E_{3i}-E_{2i})A_{s(l-i)}-\vec{I}_1\bullet\sum_{j=I-4}^{4}B_{sj}\overline{CE}_{I-j},\quad l=0,1,...,8$$

$$B_{tz}=\sum_{i=z-6}^{2}(D_{2i}-D_{3i})A_{s(z-i)}-\vec{I}_1\bullet\sum_{j=z-4}^{4}B_{sj}\overline{DC}_{z-j},\quad z=0,1,...,8$$

$$A_q=\vec{I}_1\bullet\sum_{j=q-4}^{6}A_{sj}\overline{DE}_{q-j},\quad q=0,1,...,10$$

$$\overrightarrow{DE}_n=\begin{cases}\sum_{j=n-2}^{2}\vec{d}_j\times\vec{e}_{n-j}, & n=0,1,\cdots,4\\ 0, & n<0\end{cases},$$

$$\overrightarrow{CE}_n=\begin{cases}\sum_{j=n-2}^{2}\vec{c}_j\times\vec{e}_{n-j}, & n=0,1,\cdots,4\\ 0, & n<0\end{cases}$$

$$\overrightarrow{DC}_n=\begin{cases}\sum_{j=n-2}^{2}\vec{d}_j\times\vec{c}_{n-j}, & n=0,1,\cdots,4\\ 0, & n<0\end{cases},$$

$$\vec{c}_j=\begin{cases}(C_{1j},\ C_{2j},\ C_{3j}), & j=0,1,2\\ 0, & j<0\end{cases}$$

$$\vec{d}_j=\begin{cases}(D_{1j},\ D_{2j},\ D_{3j}), & j=0,1,2\\ 0, & j<0\end{cases},$$

$$\vec{e}_j=\begin{cases}(E_{1j},\ E_{2j},\ E_{3j}), & j=0,1,2\\ 0, & j<0\end{cases}$$

$\mathbf{0}=(0,\ 0,\ 0)$, $\vec{I}_1=(1,\ 0,\ 0)$, $\vec{I}=(1,\ 1,\ 1)$

Employing Eqs. (12)-(14) and taking $S_0=\left[\ddot{X}_g(\mathrm{i}\omega)\right]\left[\ddot{X}_g(-\mathrm{i}\omega)\right]$ into consideration, in which s_0 is the intensity of the white noise, the second-order moments of displacements (i.e., displacement variances) of the structure with the attached ATTMD, ATMD1, and ATMD2 can be evaluated, respectively by following expression

$$\begin{aligned}\sigma_{y_s}^2&=\int_{-\infty}^{+\infty}\left[Y_s(\mathrm{i}\omega)\right]\left[Y_s(-\mathrm{i}\omega)\right]d\omega=\int_{-\infty}^{+\infty}\left[G_s(\mathrm{i}\omega)\right]\left[G_s(-\mathrm{i}\omega)\right]\left[\ddot{X}_g(\mathrm{i}\omega)\right]\left[\ddot{X}_g(-\mathrm{i}\omega)\right]d\omega\\&=S_0\int_{-\infty}^{+\infty}\left[G_s(\mathrm{i}\omega)\right]\left[G_s(-\mathrm{i}\omega)\right]d\omega\\&=S_0\omega_s\int_{-\infty}^{+\infty}\left[\frac{\sum_{r=0}^{4}B_{sr}(\mathrm{i}\lambda)^r}{\omega_s^2\sum_{p=0}^{6}A_{sp}(\mathrm{i}\lambda)^p}\right]\left[\frac{\sum_{r=0}^{4}B_{sr}(-\mathrm{i}\lambda)^r}{\omega_s^2\sum_{p=0}^{6}A_{sp}(-\mathrm{i}\lambda)^p}\right]d\lambda\\&=S_0\frac{1}{\omega_s^3}\int_{-\infty}^{+\infty}\frac{g_{s6}(\mathrm{i}\lambda)}{\left[h_{s6}(\mathrm{i}\lambda)\right]\left[h_{s6}(-\mathrm{i}\lambda)\right]}d\lambda\end{aligned} \tag{15}$$

$$\begin{aligned}\sigma_{y1}^2&=\int_{-\infty}^{+\infty}\left[Y_1(\mathrm{i}\omega)\right]\left[Y_1(-\mathrm{i}\omega)\right]d\omega\\&=\int_{-\infty}^{+\infty}\left[G_1(\mathrm{i}\omega)\right]\left[G_1(-\mathrm{i}\omega)\right]\left[\ddot{X}_g(\mathrm{i}\omega)\right]\left[\ddot{X}_g(-\mathrm{i}\omega)\right]d\omega\\&=S_0\int_{-\infty}^{+\infty}\left[G_1(\mathrm{i}\omega)\right]\left[G_1(-\mathrm{i}\omega)\right]d\omega\\&=S_0\omega_s\int_{-\infty}^{+\infty}\left[\frac{\sum_{l=0}^{8}B_{Tl}(\mathrm{i}\lambda)^l}{\omega_s^2\sum_{q=0}^{10}A_q(\mathrm{i}\lambda)^q}\right]\left[\frac{\sum_{l=0}^{8}B_{Tl}(-\mathrm{i}\lambda)^l}{\omega_s^2\sum_{q=0}^{10}A_q(-\mathrm{i}\lambda)^q}\right]d\lambda\\&=S_0\frac{1}{\omega_s^3}\int_{-\infty}^{+\infty}\frac{g_{T10}(\mathrm{i}\lambda)}{\left[h_{10}(\mathrm{i}\lambda)\right]\left[h_{10}(-\mathrm{i}\lambda)\right]}d\lambda\end{aligned} \tag{16}$$

$$\begin{aligned}\sigma_{y2}^2&=\int_{-\infty}^{+\infty}\left[Y_2(\mathrm{i}\omega)\right]\left[Y_2(-\mathrm{i}\omega)\right]d\omega\\&=\int_{-\infty}^{+\infty}\left[G_2(\mathrm{i}\omega)\right]\left[G_2(-\mathrm{i}\omega)\right]\left[\ddot{X}_g(\mathrm{i}\omega)\right]\left[\ddot{X}_g(-\mathrm{i}\omega)\right]d\omega\\&=S_0\int_{-\infty}^{+\infty}\left[G_2(\mathrm{i}\omega)\right]\left[G_2(-\mathrm{i}\omega)\right]d\omega\\&=S_0\omega_s\int_{-\infty}^{+\infty}\left[\frac{\sum_{z=0}^{8}B_{tz}(\mathrm{i}\lambda)^z}{\omega_s^2\sum_{q=0}^{10}A_q(\mathrm{i}\lambda)^q}\right]\left[\frac{\sum_{z=0}^{8}B_{tz}(-\mathrm{i}\lambda)^z}{\omega_s^2\sum_{q=0}^{10}A_q(-\mathrm{i}\lambda)^q}\right]d\lambda\\&=S_0\frac{1}{\omega_s^3}\int_{-\infty}^{+\infty}\frac{g_{t10}(\mathrm{i}\lambda)}{\left[h_{10}(\mathrm{i}\lambda)\right]\left[h_{10}(-\mathrm{i}\lambda)\right]}d\lambda\end{aligned} \tag{17}$$

where

$$g_{s6}(\mathrm{i}\lambda)=\sum_{r=0}^{6-1}b_{sr}(\mathrm{i}\lambda)^{2(6-1-r)},\quad h_{s6}(\mathrm{i}\lambda)=\sum_{p=0}^{6}a_{sp}(\mathrm{i}\lambda)^{6-p}$$

$$g_{T10}(\mathrm{i}\lambda)=\sum_{l=0}^{10-1}b_{Tl}(\mathrm{i}\lambda)^{2(10-1-l)},\quad g_{t10}(\mathrm{i}\lambda)=\sum_{z=0}^{10-1}b_{tz}(\mathrm{i}\lambda)^{2(10-1-z)},$$

$$h_{10}(\mathrm{i}\lambda)=\sum_{q=0}^{10}a_q(\mathrm{i}\lambda)^{10-q}$$

$$a_{sp}=A_{s(6-p)},\quad p=0,1,2,\cdots,6$$

$$a_q=A_{(10-q)},\quad q=0,1,2,\cdots,10$$

$$b_{sr}=\begin{cases}0, & r=0\\ (-1)^{r-1}B_{s(5-r)}{}^2+2\sum_{n=2}^{3-|r-3|}(-1)^{r-n}B_{s(6-r-n)}B_{s(4-r+n)}, & r=1,2,\cdots,5\end{cases}$$

$$b_{Tl}=\begin{cases}0, & l=0\\ (-1)^{l-1}B_{T(9-l)}{}^2+2\sum_{n=2}^{5-|l-5|}(-1)^{l-n}B_{T(10-l-n)}B_{T(8-l+n)}, & l=1,2,\cdots,9\end{cases}$$

$$b_{tz}=\begin{cases}0, & z=0\\ (-1)^{z-1}B_{t(9-z)}{}^2+2\sum_{n=2}^{5-|z-5|}(-1)^{z-n}B_{t(10-z-n)}B_{t(8-z+n)}, & z=1,2,\cdots,9\end{cases}$$

Further, the dimensionless displacement variance for the structure with the attached ATTMD can be determined in

Table 1 Respective coefficients of Eqs. (9)-(11)

Equations	Coefficients		
(9)	$C_{12}=1-\alpha_1\mu_1-\alpha_1\mu_2$	$C_{11}=2\xi_s$	$C_{10}=1$
	$D_{12}=0$	$D_{11}=-2\xi_1\mu_1 f_1$	$D_{10}=-\mu_1 f_1^2$
	$E_{12}=0$	$E_{11}=-2\xi_2\mu_2 f_2$	$E_{10}=-\mu_2 f_2^2$
(10)	$C_{22}=1+\alpha_1$	$C_{21}=0$	$C_{20}=0$
	$D_{22}=1$	$D_{21}=2\xi_1 f_1+\xi_T\frac{1+\eta}{\eta}(f_1+f_2)$	$D_{20}=f_1^2$
	$E_{22}=0$	$E_{21}=-\xi_T\frac{1+\eta}{\eta}(f_1+f_2)$	$E_{20}=0$
(11)	$C_{32}=1+\alpha_2$	$C_{31}=0$	$C_{30}=0$
	$D_{32}=0$	$D_{31}=-\xi_T(1+\eta)(f_1+f_2)$	$D_{30}=0$
	$E_{32}=1$	$E_{31}=2\xi_2 f_2+\xi_T(1+\eta)(f_1+f_2)$	$E_{30}=f_2^2$

the form (Spanos 1983)

$$R_{H_s}=\frac{\omega_s^3}{2\pi S_0}\sigma_{y_s}^2=\frac{I_6}{2\pi} \tag{18}$$

The dimensionless displacement variance for ATMD1 in ATTMD may be represented as

$$R_{H_1}=\frac{1}{500}\left(\frac{\omega_s^3}{2\pi S_0}\sigma_{y_1}^2\right)=\frac{I_{10}}{1000\pi} \tag{19}$$

And likewise, the dimensionless displacement variance for ATMD2 in ATTMD is computed as

$$R_{H_2}=\frac{1}{500}\left(\frac{\omega_s^3}{2\pi S_0}\sigma_{y2}^2\right)=\frac{I_{10}^{'}}{1000\pi} \tag{20}$$

Herein, the scaling coefficient of 1/500 introduced in Eqs. (19) and (20) is to take into consideration the convenience of drawing. The calculations of I_6, I_{10}, and $I_{10}^{'}$ in Eqs. (19)-(20) are detailed in Table 2.

3. Optimum performance of ATTMD in the frequency domain

This section focuses on evaluating the optimum performance of ATTMD in the frequency domain, including both the optimization and performance evaluation. Fig. 2 presents the framework for evaluating the optimum performance of ATTMD in the frequency domain.

3.1 Gradient method based optimization of ATTMD

The four variables (f_1, f_2, ξ_1, and ξ_2) to be optimized as well as their respective incremental intervals (Δf_1, Δf_2, $\Delta\xi_1$, and $\Delta\xi_2$) are listed in Table 3. The mass ratio of the ATMD1 to the structure (μ_1) is known as the smaller mass ratio (SMR), whereas the mass ratio of the ATMD2 to the structure (μ_2) is called the larger mass ratio (LMR), yet the ratio of the SMR to LMR is named as η. Likewise, in order to seek to find the optimum SMR, the various values of η are taken into consideration in the numerical analysis. The α_1 and α_2 are the normalized acceleration feedback gain factors (NAFGF) of both the ATMD1 and ATMD2, respectively. The ratio between α_1 and α_2 is designated as γ. In order to deploy control forces on the ATMD1 and ATMD2, the different values of γ are singled out. And more importantly, in order to provide valuable insight into the sensitivity of the ATTMD to the linking damping ratio ξ_T between the ATMD1 and ATMD2, its diverse values are taken into account and served as the abscissa of all the graphs. The total mass ratio μ_T and total normalized acceleration feedback gain factor α_T of the ATTMD are, respectively, equal to $\mu_1+\mu_2$ and $\alpha_1+\alpha_2$, in parallel to defining the SMR, LMR, and NAFGF. The assigned values

Table 2 Calculations of I_6, I_{10}, and $I_{10}^{'}$ in Eqs. (18)-(20)

Equations	Coefficients	
(18)	$I_6=I_m$ (i.e., m=6)	$b_{m-i}^*=(-1)^{m-i}b_{s(i-1)},\ i=1,2,3,\cdots,m\quad a_j^*=a_{sj},\ j=0,1,2,\cdots,m$
(19)	$I_{10}=I_m$ (i.e., m=10)	$b_{m-i}^*=(-1)^{m-i}b_{T(i-1)},\ i=1,2,3,\cdots,m$ $a_j^*=a_j,\ j=0,1,2,\cdots,m$
(20)	$I_{10}^{'}=I_m$ (i.e., m=10)	$b_{m-i}^*=(-1)^{m-i}b_{t(i-1)},\ i=1,2,3,\cdots,m$ $a_j^*=a_j,\ j=0,1,2,\cdots,m$
General form (Spanos 1983)	$I_m=\sum_{i=1}^{m}b_{m-i}^*M_{2(m-i)}$	$P_m=\begin{vmatrix} a_1^* & -a_3^* & a_5^* & -a_7^* & \cdots & . & . & . \\ -a_0^* & a_2^* & -a_4^* & a_6^* & \cdots & . & . & . \\ 0 & -a_1^* & a_3^* & -a_5^* & \cdots & . & . & . \\ 0 & a_0^* & -a_2^* & a_4^* & \cdots & . & . & . \\ . & . & . & . & \cdots & . & . & . \\ 0 & 0 & 0 & 0 & \cdots & . & -a_{m-2}^* & a_m^* \end{vmatrix}$
	$M_{2(m-i)}=\bar{P}_{mi}/P_m$	$\bar{P}_{mi}=\begin{vmatrix} a_1^* & -a_3^* & a_5^* & -a_7^* & \cdots & \pi/a_0^* & . & . & . \\ -a_0^* & a_2^* & -a_4^* & a_6^* & \cdots & 0 & . & . & . \\ 0 & -a_1^* & a_3^* & -a_5^* & \cdots & 0 & . & . & . \\ 0 & a_0^* & -a_2^* & a_4^* & \cdots & 0 & . & . & . \\ . & . & . & . & \cdots & . & . & . & . \\ . & . & . & . & \cdots & . & . & -a_{m-2}^* & a_m^* \end{vmatrix}$

Table 3 Targets and ranges of explored parameters as well as assigned parameter values

μ_T=0.01		
ξ_s=0.02		
α_T=4, 8		
η=0.25, 0.50, 0.75, 1.00		
γ=1/4, 1/2, 1, 2, 4		
f_1 (To be optimized)	$0 \le f_1 \le 2.0$	Δf_1=0.001
f_2 (To be optimized)	$0 \le f_2 \le 2.0$	Δf_2=0.001
ξ_1 (To be optimized)	$0 \le \xi_1 \le 0.999$	$\Delta \xi_1$=0.001
ξ_2 (To be optimized)	$0 \le \xi_2 \le 0.999$	$\Delta \xi_2$=0.001
ξ_T=0.0, 0.1, 0.2, 0.3, 0.4		

of μ_T, α_T, η, γ, ξ_T, and ξ_s (the modal damping ratio of structures) are presented in Table 3.

Since in the present work the focus is on the protection, i.e., taking into account the structural integrity and safety, of the civil engineering structure by reducing its displacement response, the objective function is defined as the dimensionless displacement variances of the structure with the attached ATTMD. Naturally, this objective function can measure the ATTMD performance and its minimization will lead to the corresponding optimal parameters of the ATTMD system. Likewise, the lower the value of the objective function, the higher the effectiveness of the ATTMD. In order to identify the optimal parameter values of the ATTMD system, a gradient-based searching technique in MATLAB software platform shown in Fig. 2 is taken into consideration. Due to the closed-form expression of the objective function, this optimization technique is capable of making precise determination on the ATTMD parameters.

Here, it is especially pointed out that in the following graphs min.R_{Hs} denotes the minimum values of the dimensionless displacement variances of the structure coupled with the ATTMD; $f_{1\ opt}$ and $\xi_{1\ opt}$ represent the optimum tuning frequency ratio and the optimum damping ratio of the ATMD1, respectively; $f_{2\ opt}$ and $\xi_{2\ opt}$ refer to the optimum tuning frequency ratio and the optimum damping ratio of the ATMD2, respectively; and, R_{H1} and R_{H2} are the normalized values of the dimensionless displacement variances of both the ATMD1 and ATMD2 taking their respective optimum parameters.

In the physical sense, min.R_{Hs} is used to measure the

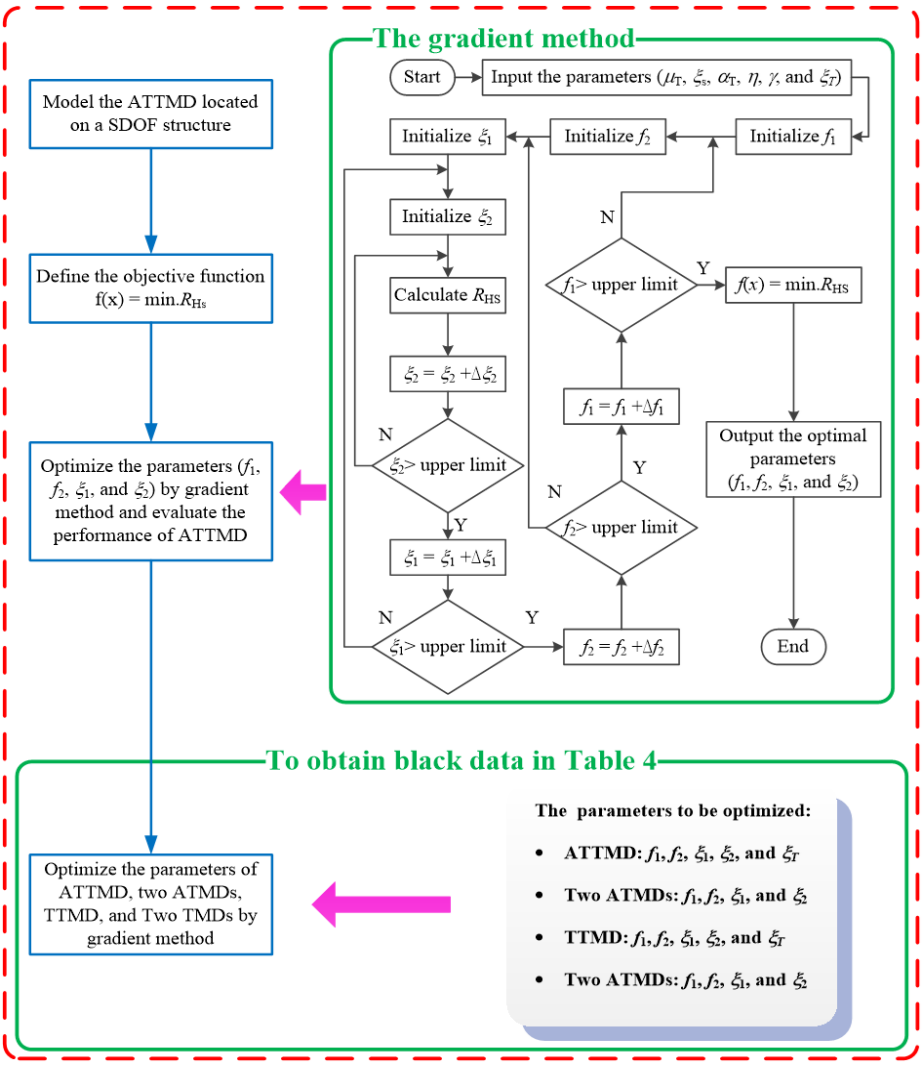

Fig. 2 Framework for evaluating the optimum performance of ATTMD in the frequency domain

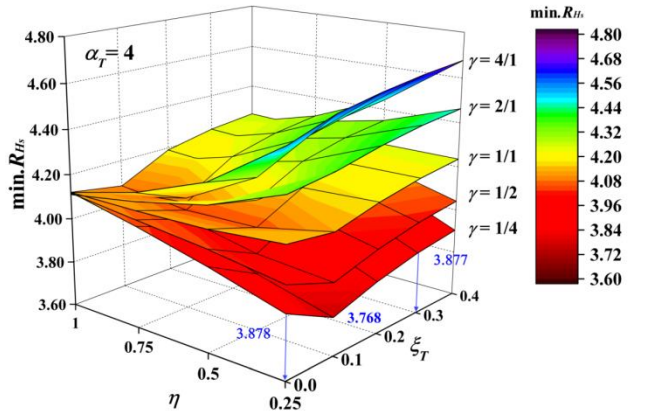

Fig. 3 Three-dimensional min.R_{Hs} surface used for measuring the effectiveness of the ATTMD with reference to given ratio of the SMR to LMR (η) and linking damping ratio (ξ_τ) under α_T=4.0

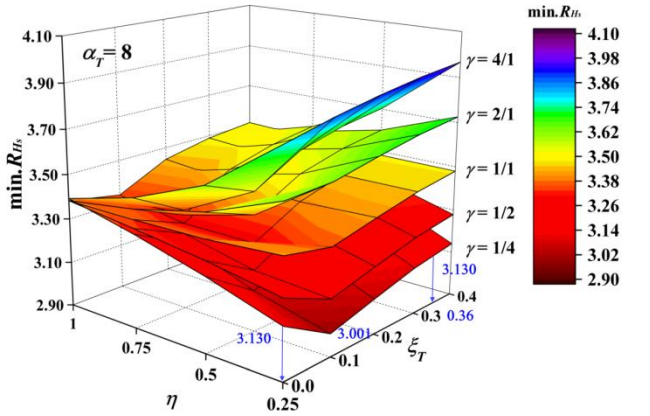

Fig. 4 Three-dimensional min.R_{Hs} surface used for measuring the effectiveness of the ATTMD with reference to given ratio of the SMR to LMR (η) and linking damping ratio (ξ_τ) under α_T=8.0.

effectiveness of the ATTMD, while R_{H1} and R_{H2} are harnessed to evaluate the relative magnitude of the strokes of both the ATMD1 and ATMD2 in the ATTMD. Likewise, analogous to the ATTMD, the objective functions of two ATMDs, two TMDs, and the TTMD are also to minimize the dimensionless displacement variances of the structures coupled with them in order to guarantee the structural integrity. By resorting to these objective functions and gradient-based searching technique, the results of min.R_{Hs}, R_{H1}, R_{H2}, and the optimum parameters will be exhibited and analysed next in detail.

3.2 Estimating the performance of ATTMD

The performance of ATTMD will be scrutinized through analysing and comparing the effectiveness, optimum tuning frequency ratio, optimum frequency spacing, optimum damping ratio, and stroke.

3.2.1 Effectiveness

The plot of three-dimensional min.R_{Hs} surface is displayed in Fig. 3 used for measuring the effectiveness of the ATTMD with reference to given ratio of the SMR to LMR (η) and linking damping ratio (ξ_τ) under α_T=4.0, whereas under α_T=8.0 is shown is in Fig. 4.

It can be seen from Fig. 3 that for different values of η, the variation trends of min.R_{Hs} are very similar with the linking damping ratio. Decreasing in the effectiveness of the ATTMD may be observed for increasing the values of γ, such as the case of η=0.25; but overall, this decreasing trend is becoming less and less obvious with the decrease of η, such as the case of η=1.0. From three data superposed in the Fig. 3, the optimum effectiveness of the ATTMD can be discerned at the linking damping ratio of 0.1. Interestingly, increasing the values of η and γ leads to decreasing the effectiveness of the ATTMD, thus effectively meaning that the combination of η=0.25 and γ=1/4 can bring about the optimum effectiveness of the ATTMD. A possible explanation for this phenomenon is that both the mass distribution and the linking dashpot have influences on the dynamic characteristics of the ATMD1 and ATMD2. Whether it is the ATTMD or two ATMDs, the difference between the dynamic characteristic of the ATMD1 and that of ATMD2 becomes more remarkable under a greater distinction of their mass. Likewise, viscosity of the linking dashpot will further amplify this difference when the linking damping ratio attains its optimality. Therefore, according to the different dynamic characteristics between the ATMD1 and ATMD2, the ATTMD system may be driven to the states of optimal effectiveness through deploying the suitable control forces. Notwithstanding the existence of the optimum effectiveness, given a total mass ratio and a normalized acceleration feedback gain factor (NAFGF), an accessible region of the linking damping ratio of the ATTMD with the nearly identical level of effectiveness can be easily identified, such as the range from 0.0 to 0.3 for μ_T=0.01 and α_T=4.0. In case of the total normalized acceleration feedback gain factor (α_T) of 8.0, Fig. 4 brings to light the analogous attribute to Fig. 3, along with increasing in the effectiveness of the ATTMD with increases α_T.

For further comparison purposes, Table 4 summarizes the optimum parameters, effectiveness, and optimum frequency spacing of the ATTMD and TTMD with different linking damping ratios as well as two ATMDs and two TMDs. Table 4 clearly shows that the ATTMD and two ATMDs without the dashpot possesses the nearly identical level of effectiveness, but remarkably higher than that of the passive counterparts of both the former and latter.

3.2.2 Optimum tuning frequency ratio

The graphs of variation trends of the optimum tuning frequency ratio of the ATMD1 in the ATTMD with regard to the linking damping ratio are presented in Fig. 5 with the changing of several important parameters for α_T=4.0, whereas for α_T=8.0 are demonstrated is in Fig. 6. It can be identified from Figs. 5 and 6 that for η=0.25 and η=0.5, the optimum tuning frequency ratio of the ATMD1 increases with the increasing in the linking damping ratio. For η=0.75 and η=1.0, however, the optimum tuning frequency ratio of the ATMD1 takes on the complex variation trends. Likewise, the ATTMD with the combination of η=0.25 and

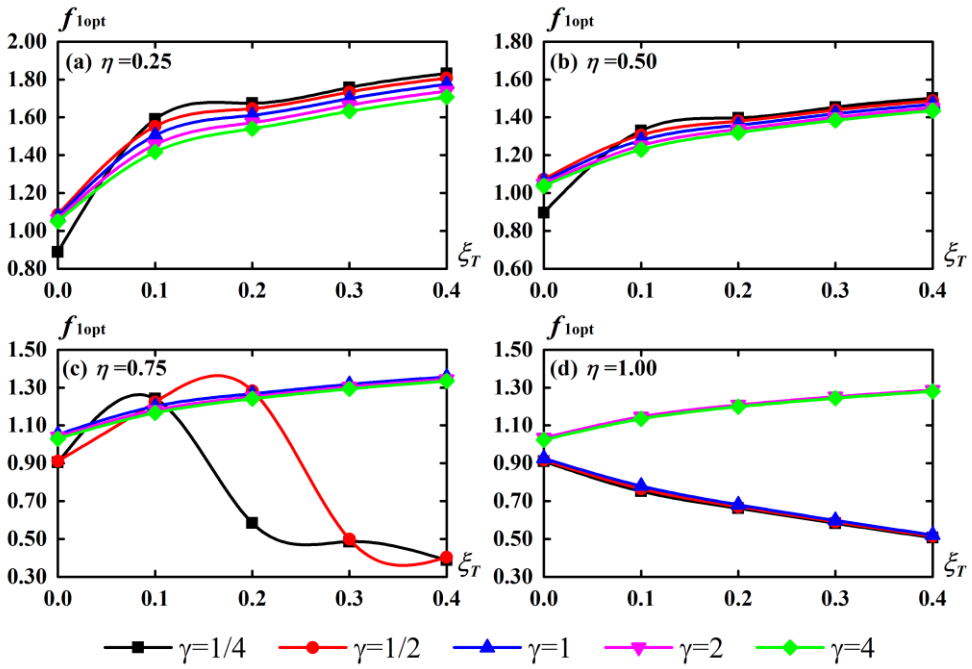

Fig. 5 Variation trends of the optimum tuning frequency ratio of the ATMD1 with regard to linking damping ratio under α_T=4.0 and under the circumstances of consecutively chosen values: (a) η=0.25, (b) η=0.5, (c) η=0.75, and (d) η=1.0

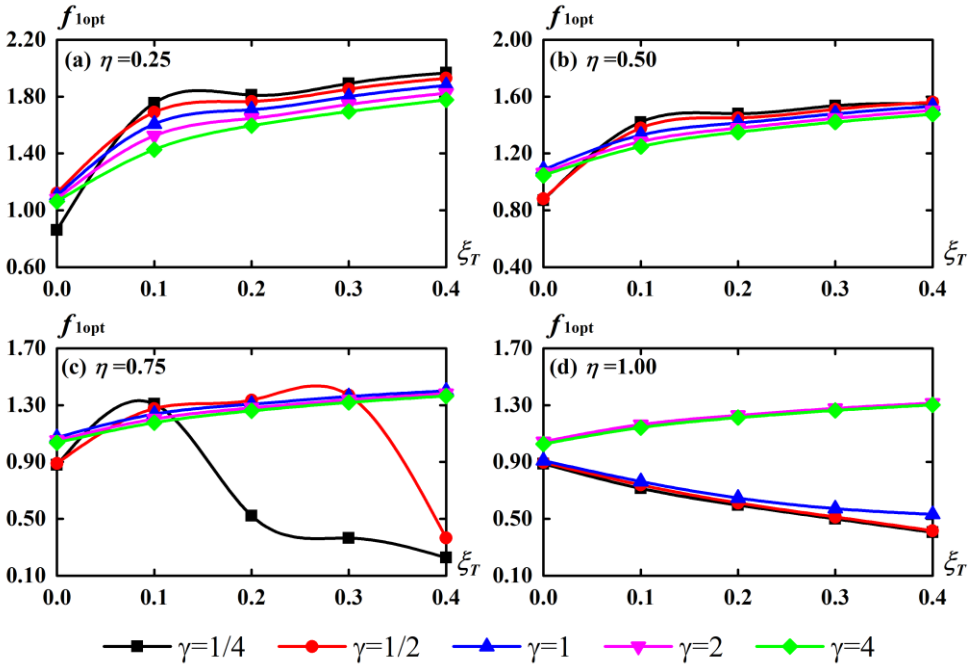

Fig. 6 Variation trends of the optimum tuning frequency ratio of the ATMD1 with regard to linking damping ratio under α_T=8.0 and under the circumstances of consecutively chosen values: (a) η=0.25, (b) η=0.5, (c) η=0.75, and (d) η=1.0

γ=1/4 has a higher optimum tuning frequency ratio of the ATMDI.

Next, the graphs of variation trends of the optimum tuning frequency ratio of the ATMD2 in the ATTMD with respect to the linking damping ratio are reported in Fig. 7 with the changing of several important parameters for α_T=4.0, whereas for α_T=8.0 are provided is in Fig. 8. It can be discerned from Figs. 7 and 8 that for η=0.25 and η=0.5, the optimum tuning frequency ratio of the ATMD2 decreases with the increasing in the linking damping ratio. Simultaneously, it is interesting to find that in general the optimum tuning frequency ratio of the ATMD2 is insensitive to the values of γ. Analogously, for η=0.75 and η=1.0 the optimum tuning frequency ratio of the ATMD2 also takes on the complex variation trends and thus, cannot be concluded in a single simple trend.

The complex variation trends may arise from a difference between the dynamic characteristic of the

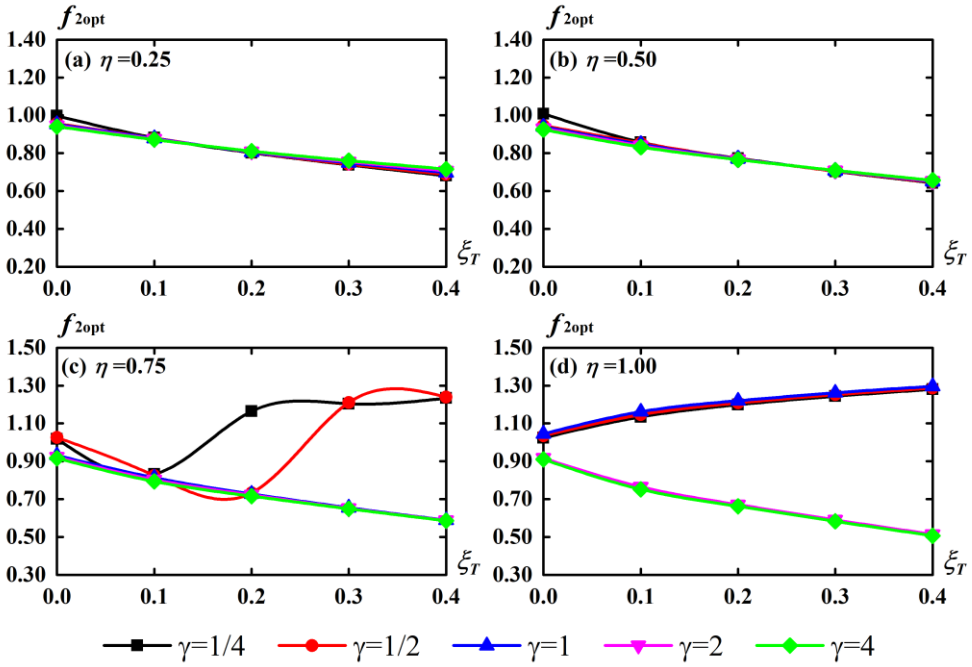

Fig. 7 Variation trends of the optimum tuning frequency ratio of the ATMD2 with regard to linking damping ratio under α_T=4.0 and under the circumstances of consecutively chosen values: (a) η=0.25, (b) η=0.5, (c) η=0.75, and (d) η=1.0

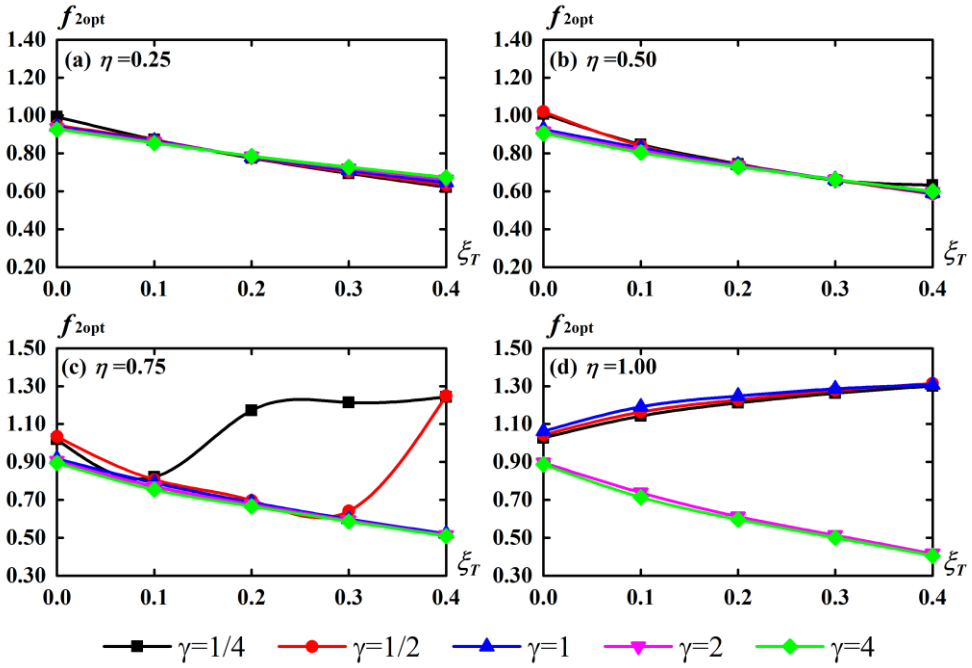

Fig. 8 Variation trends of the optimum tuning frequency ratio of the ATMD2 with regard to linking damping ratio under α_T=8.0 and under the circumstances of consecutively chosen values: (a) η=0.25, (b) η=0.5, (c) η=0.75, and (d) η=1.0

ATMD1 and that of ATMD2, which is caused by the combined effects of ξ_T, γ, and η. An augment of the linking damping ratio further widens the gap between the frequencies, while the value of each frequency decreases with the increasing of γ. Whether the ATTMD or two ATMDs, the optimization always tends to arrange the natural frequency of the ATMD2 with a heavier mass more near that of a structure so as to attenuate the response of the structure more effectively. Looking at Figs. 5-8, for the optimum tuning frequency ratios there is actually a regular tendency, that the optimum natural frequency of the ATMD2 is closer to that of a structure than the ATMD1, in spite of existence of the complex variation trends. But it brings about a sensitivity in the allocation of the tuning frequency ratios that the mass of the ATMD2 is approximate to that of the ATMD1 when η=0.75 and η=1.0, thus meaning that neither η=0.75 nor η=1.0 is an appropriate choice.

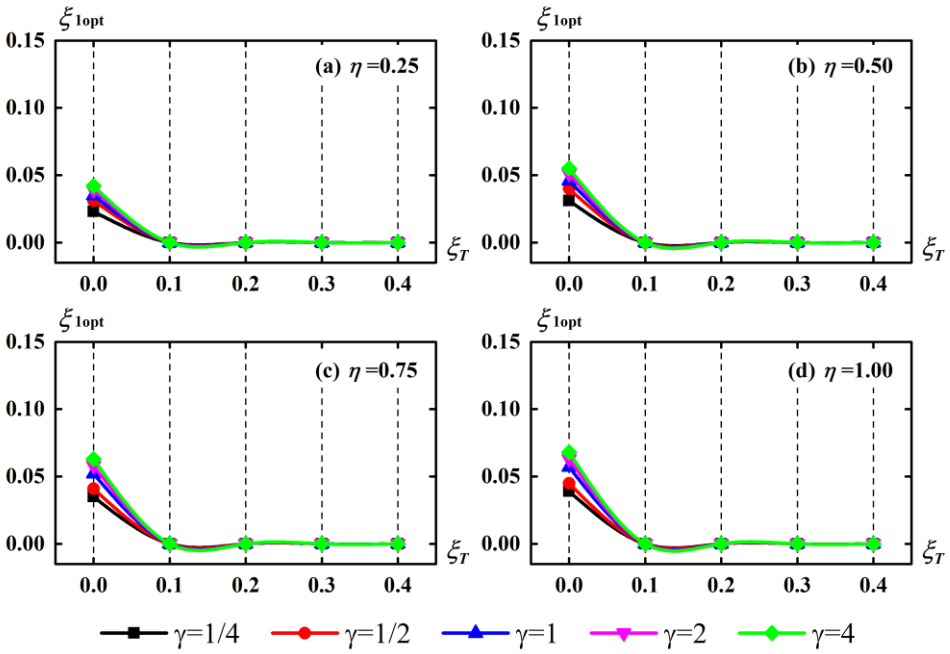

Fig. 9 Variation trends of the optimum damping ratio of the ATMD1 with respect to linking damping ratio under α_T=4.0 and under the circumstances of consecutively chosen values: (a) η=0.25, (b) η=0.5, (c) η=0.75, and (d) η=1.0

Table 4 The optimum parameters, optimum frequency spacing, and effectiveness of ATTMD and TTMD with different linking damping ratios as well as two ATMDs and two TMDs when μ_T=0.01 and η=0.25

		ξ_T	f_1	f_2	β	min.R_{Hs}
ATTMD	α_T=4 γ=1/4	0.100	1.590	0.881	0.574	3.768
		0.200	1.674	0.802	0.704	3.832
		0.093	**1.586**	**0.888**	**0.564**	**3.767**
	α_T=8 γ=1/4	0.100	1.755	0.873	0.671	3.001
		0.200	1.810	0.775	0.801	3.056
		0.106	**1.754**	**0.866**	**0.678**	**3.000**
Two ATMDs	α_T=4 γ=1/4	0.000	0.888	0.997	0.116	3.878
	α_T=8 γ=1/4	0.000	0.860	0.993	0.144	3.130
TTMD		0.100	1.350	0.899	0.401	6.057
		0.200	1.450	0.850	0.522	6.102
		0.006	**1.056**	**0.956**	**0.099**	**5.940**
Two TMDs		0.000	1.037	0.965	0.072	6.036

Note. Black data in this table represents the optimum parameters and effectiveness of the ATTMD corresponding to the optimum linking damping ratios (In this status, the linking damping ratio is treated as one of the variables to be optimized).

3.2.3 Optimum frequency spacing

Through re-examination of Figs. 5(a), 6(a), 7(a), and 8(a), it is a pleasure to discover that in the optimum scenarios, there is a clear difference between the optimum tuning frequency ratio of the ATMD1 and that of the ATMD2. This attribute is attributed to the remarkably different dynamic characteristics between the ATMD1 and ATMD2. In practical terms, this obvious difference between the optimum tuning frequency ratio of the ATMD1 and that of the ATMD2 signifies the existence of wider optimum frequency spacing, which can flatten the frequency response curve of a structure over the wider frequency range. The wider optimum frequency spacing of the ATTMD means the higher robustness against the change or estimation error in the structural natural frequency produced from structural complexity and material nonlinearity, such as the stiffness degeneration of a frame structure suffering from major earthquakes. Herein, the optimum frequency spacing of the ATTMD can be defined as $\beta=2\left|f_{1opt}-f_{2opt}\right|/(f_{1opt}+f_{2opt})$ [28-32]. Apparently, this constitutes the highlight of the proposed ATTMD.

Further comparison of the optimum frequency spacing in Table 4 clearly suggests that the optimum frequency spacing of the ATTMD is obviously larger than that of the TTMD and by a long way exceeds those of two ATMDs and two TMDs without the linking dashpot. Therefore, the proposed ATTMD possesses the highest robustness. Otherwise, the optimum frequency spacing of the ATTMD increases with the increasing in the normalized acceleration feedback gain factors (α_T). Furthermore, the results shown in Table 4 demonstrate that for the ATTMD, the optimum linking damping ratio leads to a slightly smaller optimum frequency spacing; whereas for the TTMD, the optimum linking damping ratio corresponds to a significantly smaller optimum frequency spacing.

3.2.4 Optimum damping ratio

The graphs of variation trends of the optimum damping ratio of the ATMD1 with regard to the linking damping ratio are depicted in Fig. 9 with the changing of several important parameters for α_T=4.0, whereas for α_T=8.0 are illustrated in Fig. 10. Next, the graphs of variation trends of the optimum damping ratio of the ATMD2 with respect to the linking damping ratio are reported in Fig. 11 with the changing of several important parameters for α_T=4.0, while

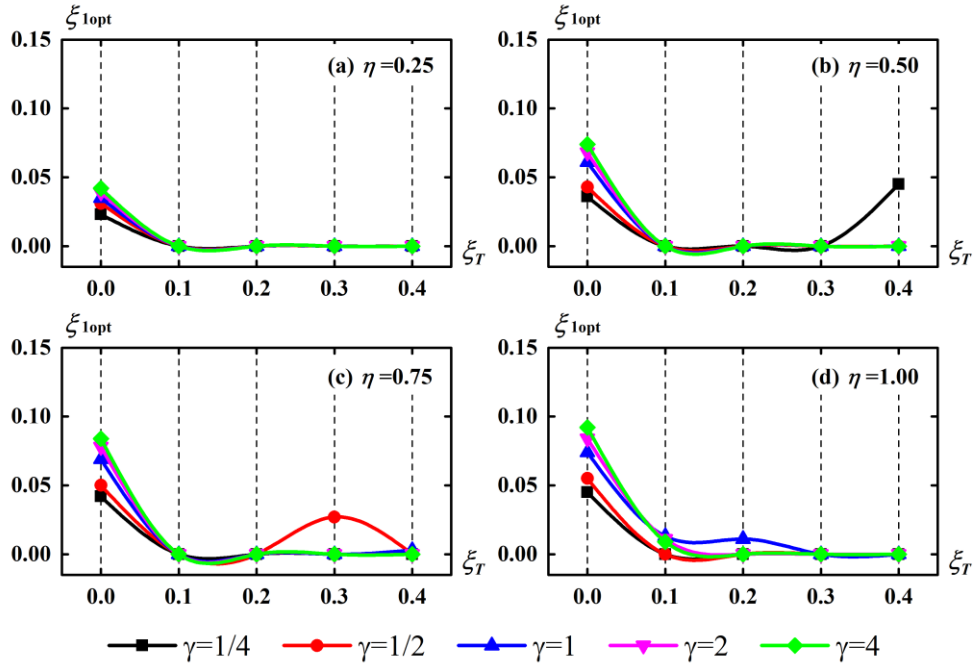

Fig. 10 Variation trends of the optimum damping ratio of the ATMD1 with respect to linking damping ratio under α_T=8.0 and under the circumstances of consecutively chosen values: (a) η=0.25, (b) η=0.5, (c) η=0.75, and (d) η=1.0

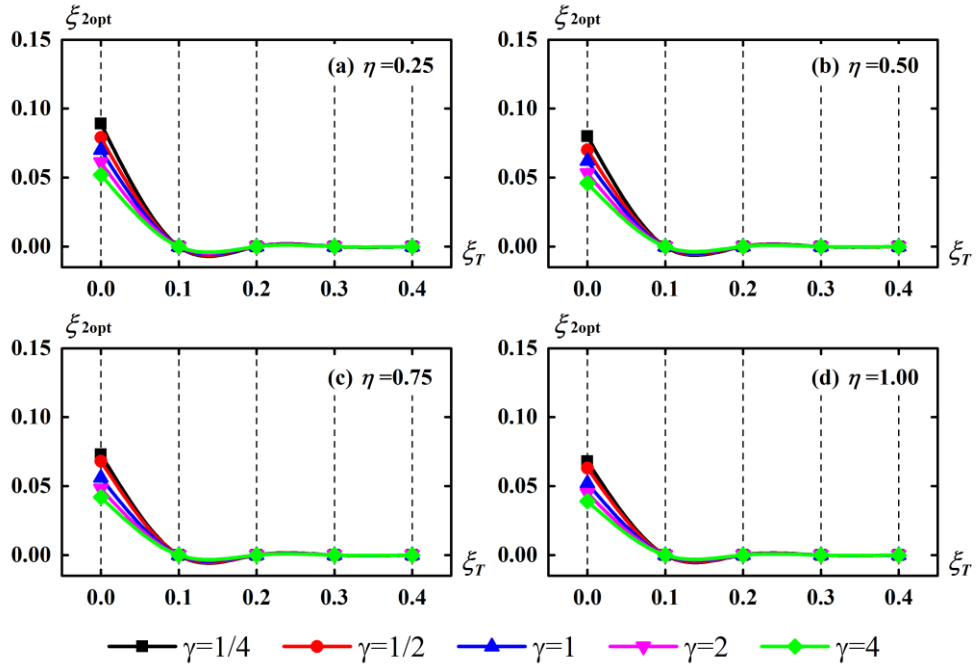

Fig. 11 Variation trends of the optimum damping ratio of the ATMD2 with respect to linking damping ratio under α_T=4.0 and under the circumstances of consecutively chosen values**:** (a) η=0.25, (b) η=0.5, (c) η=0.75, and (d) η=1.0

for α_T=8.0 are provided is in Fig. 12. From Figs. 9 and 10, it can be clearly concluded that in general the optimum damping ratio of the ATMD1 is equal to zero for different values of γ when the linking damping ratio is greater than or equal to 0.1. And likewise, it can be observed from Figs. 11 and 12 that for the optimum damping ratio of the ATMD2 there exists this feature too. The main reason that leads to no damping demand is that the dashpot of the ATMD1 and ATMD2 are localised to the linking one between them. In other words, the linking dashpot locally dissipates a significant amount of vibrational energy from the structures in lieu of those of the ATMD1 and ATMD2, so as to achieve the optimum state of the ATTMD. Here, it is remarkable to note that under the circumstances that the linking damping ratio takes its optimum values, such as 0.093 available in Table 4, instead of 0.1, analogous results can still be obtained that the optimum damping ratios of the ATMD1 and ATMD2 are simultaneously equal to zero. This feature

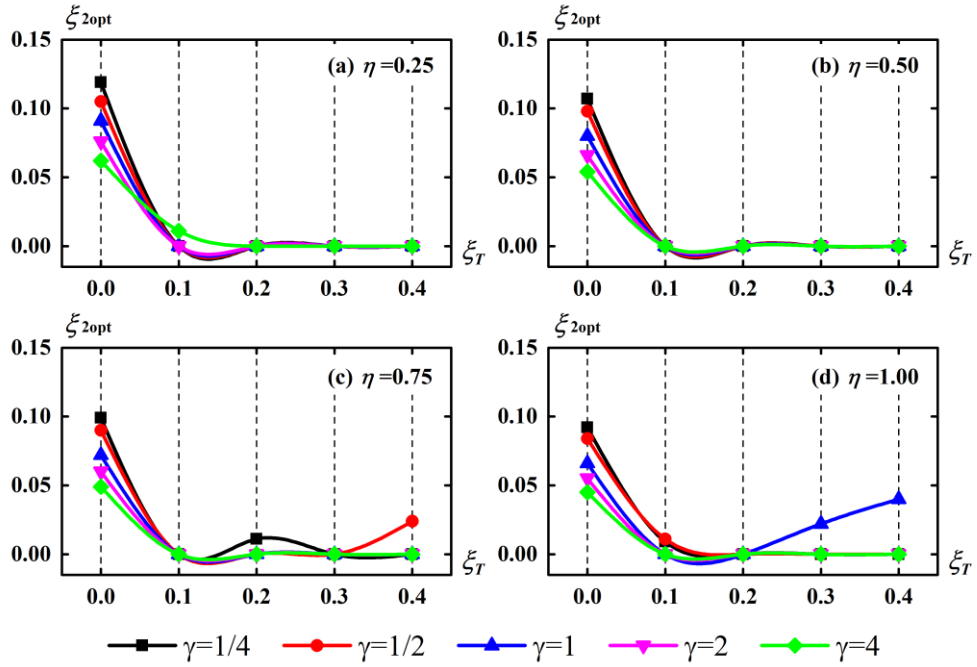

Fig. 12 Variation trends of the optimum damping ratio of the ATMD2 with respect to linking damping ratio under α_T=8.0 and under the circumstances of consecutively chosen values: (a) η=0.25, (b) η=0.5, (c) η=0.75, and (d) η=1.0

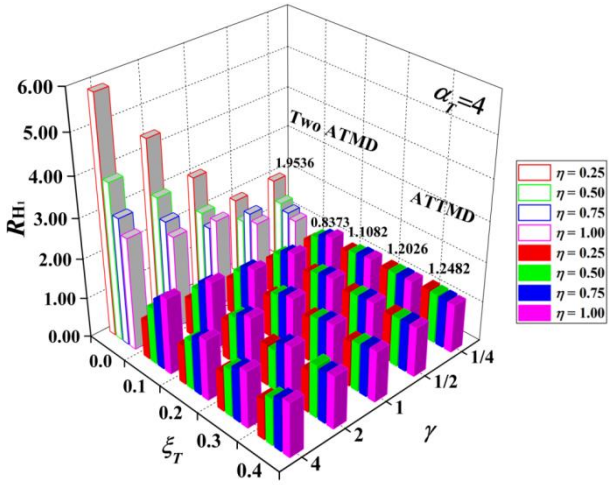

Fig. 13 Three-dimensional R_{H1} histogram of the ATMD1 with regard to given ratio of the SMR to LMR (η) and linking damping ratio (ξ_T) under α_T=4.0

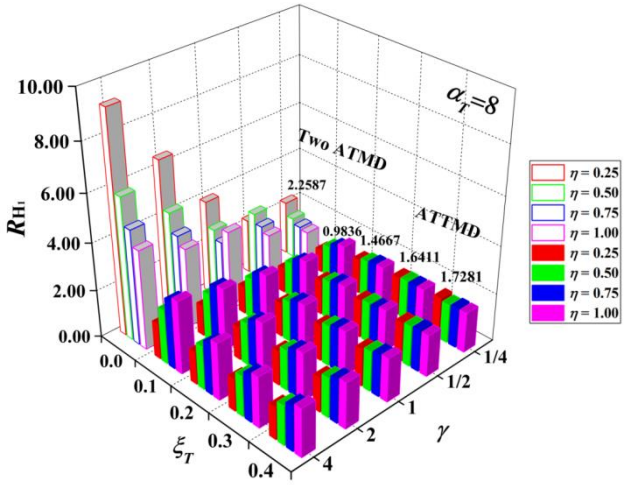

Fig. 14 Three-dimensional R_{H1} histogram of the ATMD1 with regard to given ratio of the SMR to LMR (η) and linking damping ratio (ξ_T) under α_T=8.0

manifestly simplifies the composition of the ATTMD, thereby further highlighting its simplicity and practicability for application.

3.2.5 Stroke

The variation trends of three-dimensional R_{H1} histogram, utilized for measuring the relative magnitude of the stroke of the ATMD1, with regard to given ratio of the SMR to LMR (η) and linking damping ratio (ξ_T) under α_T=4.0 and α_T=8.0 are compared in Figs. 13 and 14, and is briefly described as follows: (1) when the linking damping ratio is around 0.1, the stroke of the ATMD1 is much less than that of Two ATMDs. (2) When the linking damping ratio is equal to or greater than 0.2, the stroke of the ATMD1 cannot be further reduced. (3) The stroke of the ATMD1 is insensitive to deploying the control forces, i.e., varying the values of γ. (4) Varying the values of η does not lead to changing the variation trends of R_{H1}. (5) Smaller is the stroke of the ATMD1 in the ATTMD with the combination of η=0.25 and γ=1/4 with respect to other combinations.

Figs. 15 and 16 present the three-dimensional histograms reflecting the variation trends of R_{H2}, used for measuring the relative magnitude of the stroke of the ATMD2, with respect to given ratio of the SMR to LMR (η) and linking damping ratio (ξ_T) under α_T=4.0 and α_T=8.0. Through scrutinizing Figs. 15 and 16, the following demonstrations can be reached. The stroke of the ATMD2

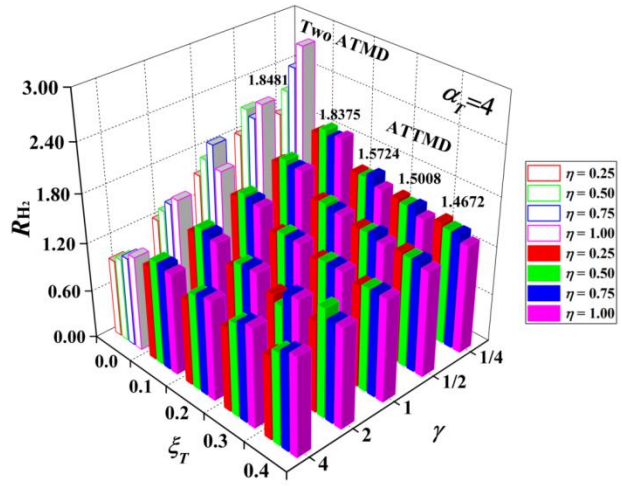

Fig. 15 Three-dimensional R_{H2} histogram of the ATMD2 with regard to given ratio of the SMR to LMR (η) and linking damping ratio (ξ_T) under α_T=4.0

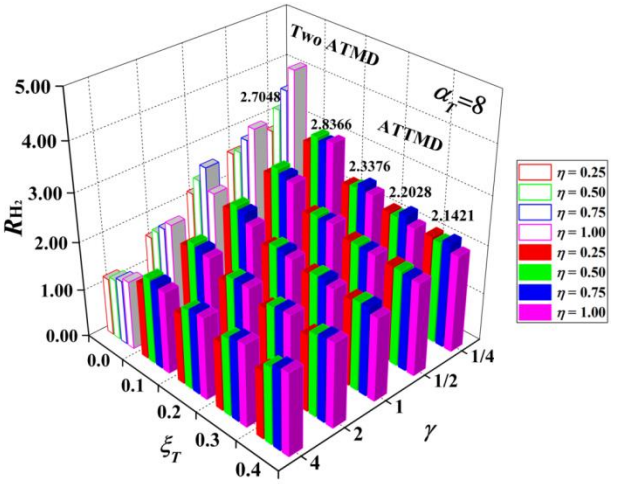

Fig. 16 Three-dimensional R_{H2} histogram of the ATMD2 with regard to given ratio of the SMR to LMR (η) and linking damping ratio (ξ_T) under α_T=8.0

decreases with the increasing in the linking damping ratio. But when the linking damping ratio is beyond ξ_T=0.2, the rate of descent of the stroke of the ATMD2 reduces. Deployment of the control forces has a certain effect on the stroke of the ATMD2. For example, for the ATTMD with the combination of η=0.25 and γ=4, the ATMD1 and ATMD2 simultaneously maintain the smaller stroke. However, it can been seen from Figs. 3 and 4 that the ATTMD with this combination provides the low level of effectiveness. Additionally, increasing the total normalized acceleration feedback gain factor (α_T) increases the stroke of the ATMD2.

In order to further delineate the effects of the linking damping ratio on the relative magnitude of the stroke of ATMD1 and ATMD2 in the ATTMD, Figs. 13-16 simultaneously present the data of R_{H1} and R_{H2} in the ATTMD with the combination of η=0.25 and γ=1/4. These data indicate clearly that the relative magnitude of the stroke of ATMD1 in the ATTMD is remarkably smaller than that of two ATMDs without a linking dashpot. Likewise, for the combination of η=0.25 and γ=1/4, in the case of α_T=8.0, the stroke of ATMD2 in the ATTMD is slightly larger than that of two ATMDs without a linking dashpot when the linking damping ratio equals 0.1. However, when the linking damping ratio is equal to or larger than 0.2, the stroke of ATMD2 in the ATTMD is smaller than that of two ATMDs.

The above phenomena are ascribed to that the linking dashpot generates a phase difference between the ATMD1 with ATMD2. This phase delay gives rise to a remarkably different dynamic characteristic between the ATMD1 and ATMD2, thereby making the linking dashpot effectively dissipate vibrational energy under an appropriate linking damping ratio. Likewise, for the ATMD1 and ATMD2, the larger the allocated NAFGF, the more vigorous its vibration. Nevertheless, the linking dashpot, with a large damping ratio, greatly suppresses their vibrations, which brings out the control effectiveness decline of the ATTMD system. Further, the linking damping ratio impacts on the strokes more heavily than the deployment of control forces. Consequently, compared with two ATMDs, the strokes of the ATMD1 and ATMD2 are less sensitive to deploying the control forces and decrease globally with the increasing of linking damping ratio.

Herein, it is worthwhile emphasizing that through analysing comprehensively on Figs. 3, 4, 13-16, increasing the linking damping ratio of the ATTMD with the combination of η=0.25 and γ=1/4 not only can reduce the stroke of the ATMD2, but also render a higher effectiveness than the combination of η=0.25 and γ=4.

4. Effectiveness and stroke verification of ATTMD in time domain

Subsequent to the frequency domain analysis, the effectiveness and stroke verification of ATTMD in the time history domain will be performed in this section. We consider a seismically excited three-storey building with a set of ATTMD or Two ATMDs installed on the top floor. The structural mass and stiffness coefficients for each storey are m_{si}=1.0198×10^5 kg and k_{si}=1.28472×10^8 N/m for i=1,2,3. The structural modal information of the three-storey building is given in the following. Natural frequencies of the three modes of the structure are ω_{s1}=15.7960 rad/s, ω_{s2}=44.2595 rad/s, ω_{s3}=63.9568 rad/s, respectively. The corresponding generalised modal masses of the structure are $m_1^*=1.87762\times10^5$ kg, $m_2^*=2.9196\times10^5$ kg, and $m_3^*=9.48\times10^5$ kg, respectively. Three damping ratios for of the three modes of the structure are assumed to be ξs_1=ξs_2=ξs_3=0.02 of the critical damping, which is modelled as Rayleigh damping. Employing Rayleigh damping, the damping matrix of the three-storey structure may be obtained through a linear combination of mass-proportional and stiffness-proportional damping terms (Erduran 2012). Three earthquake records shown in Table 5, including two actual El-Centro and Tianjin records, and one artificial Shanghai record, a synthesized ground motion using the target response spectrum in compliance with the

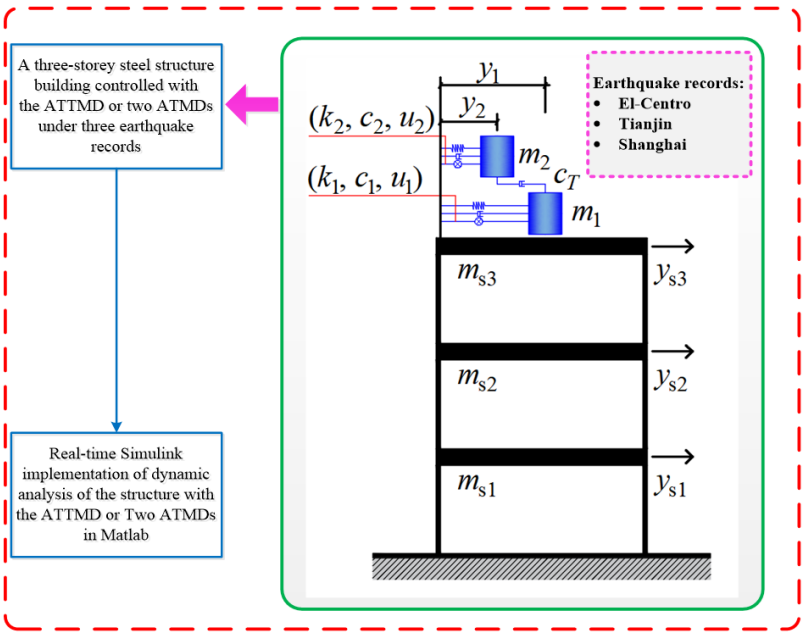

Fig. 17 Framework for effectiveness and stroke verification of ATTMD in the time history domain

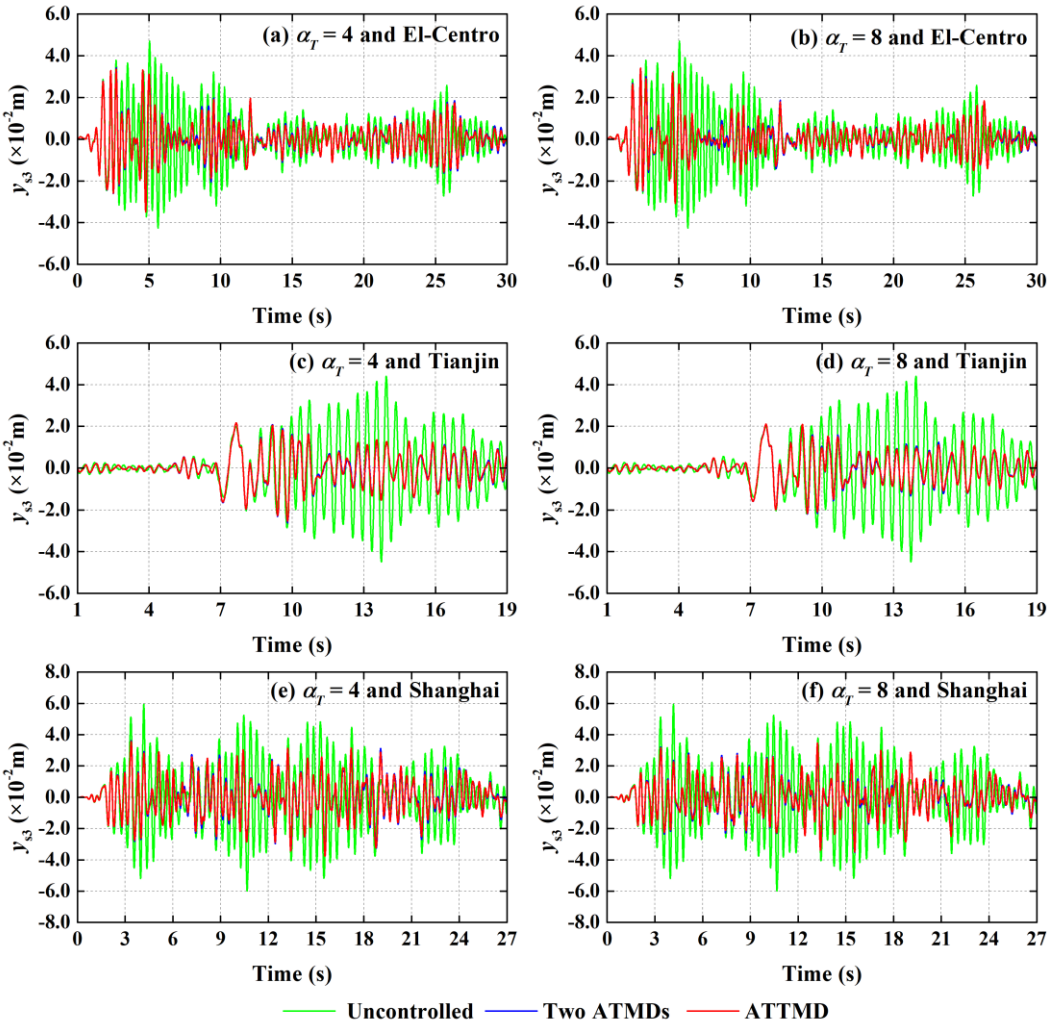

Fig. 18 Time history plots of displacement of three-storey building with and without the optimum ATTMD (taking the optimum linking damping ratio) or optimum Two ATMDs with μ_T=0.01, η=0.25, and γ=1/4 for two normalized acceleration feedback gain factors and three earthquake records: (a) α_T=4 and El-Centro, (b) α_T=8 and El-Centro, (c) α_T=4 and Tianjin, (d) α_T=8 and Tianjin, (e) α_T=4 and Shanghai, and (f) α_T=8 and Shanghai

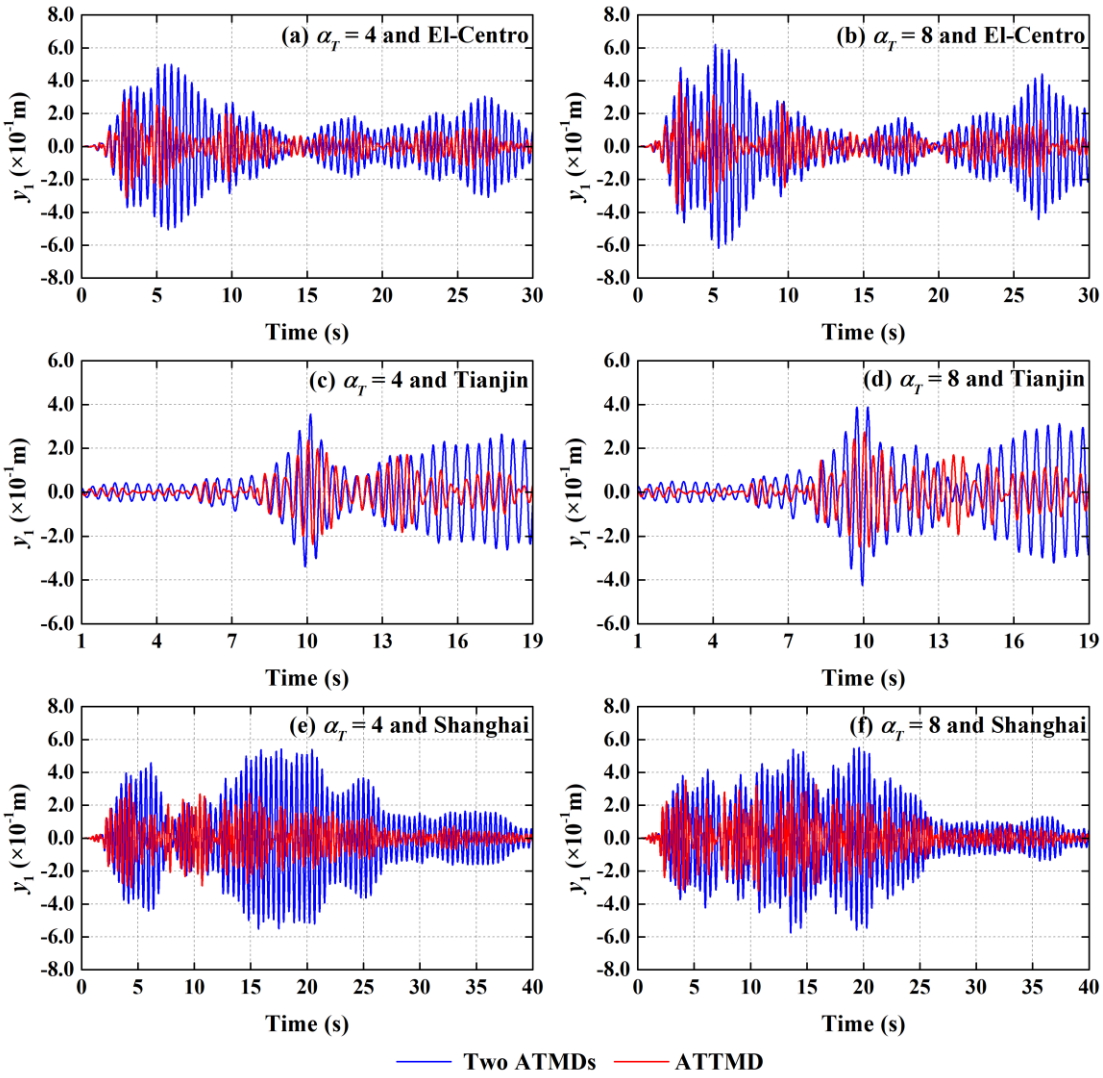

Fig. 19 Time history plots of stroke of the ATMD1 in the optimum ATTMD (taking the optimum linking damping ratio) and optimum Two ATMDs with μ_T=0.01, η=0.25, and γ=1/4 for two normalized acceleration feedback gain factors and three earthquake records: (a) α_T=4 and El-Centro, (b) α_T=8 and El-Centro, (c) α_T=4 and Tianjin, (d) α_T=8 and Tianjin, (e) α_T=4 and Shanghai, and (f) α_T=8 and Shanghai

Table 5 Characteristics of earthquake records

Earthquake Records	Name	Year	Record Station	PGA (cm/s^2)	Sampling Interval (s)	Time Range (s)	Scaled PGA
El-Centro	Imperial Valley, USA	1940	117 El-Centro	314.70	0.02	0~30	0.4 g
Tianjin	Ninhe Tianjin, CHN	1976	Tianjin Hospital	145.80	0.01	0~19	0.4 g
Shanghai	Synthesized ground motion	—	Shanghai	35.00	0.01	0~27	0.4 g

code for seismic design of buildings, are used as the input excitations in the numerical simulation. The damper mass is taken to be 1% of the first-mode generalised modal mass (i.e., μ_T=0.01). Employing the analysis results in the frequency domain, the designing parameters of investigated ATTMD and Two ATMDs with μ_T=0.01, η=0.25, and γ=1/4 are given in the Table 6. In this numerical study, two cases

Table 6 Designing parameters of investigated ATTMD and Two ATMDs with μ_T=0.01, η=0.25, and γ=1/4 in two cases of the optimum linking damping ratio (ξ_{Topt}) and ξ_T=0.2 under three earthquakes (%)

	α_T	ξ_T	$k_1+\bar{k}_1$ (N/m)	$k_2+\bar{k}_2$ (N/m)	$c_1+\bar{c}_1$ (N·s/m)	$c_2+\bar{c}_2$ (N·s/m)	c_T (N·s/m)
ATTMD	4	**0.093**	**235688.5**	**295541.1**	**0**	**0**	**6824.0**
		0.200	262568.6	241068.6	0	0	14687.1
	8	**0.106**	**288264.5**	**281078.6**	**0**	**0**	**8236.9**
		0.200	306965.2	225110.3	0	0	15333.6
Two ATMD	4	0	73885.3	372548.0	242.3	4210.8	0
	8	0	69299.3	369564.7	275.5	5607.5	0

of the optimum linking damping ratio and ξ_T=0.2 are considered, as shown in Table 6. Fig. 17 presents the framework for effectiveness and stroke verification of the ATTMD in the time history domain.

Fig. 18 presents the time history plots of displacement

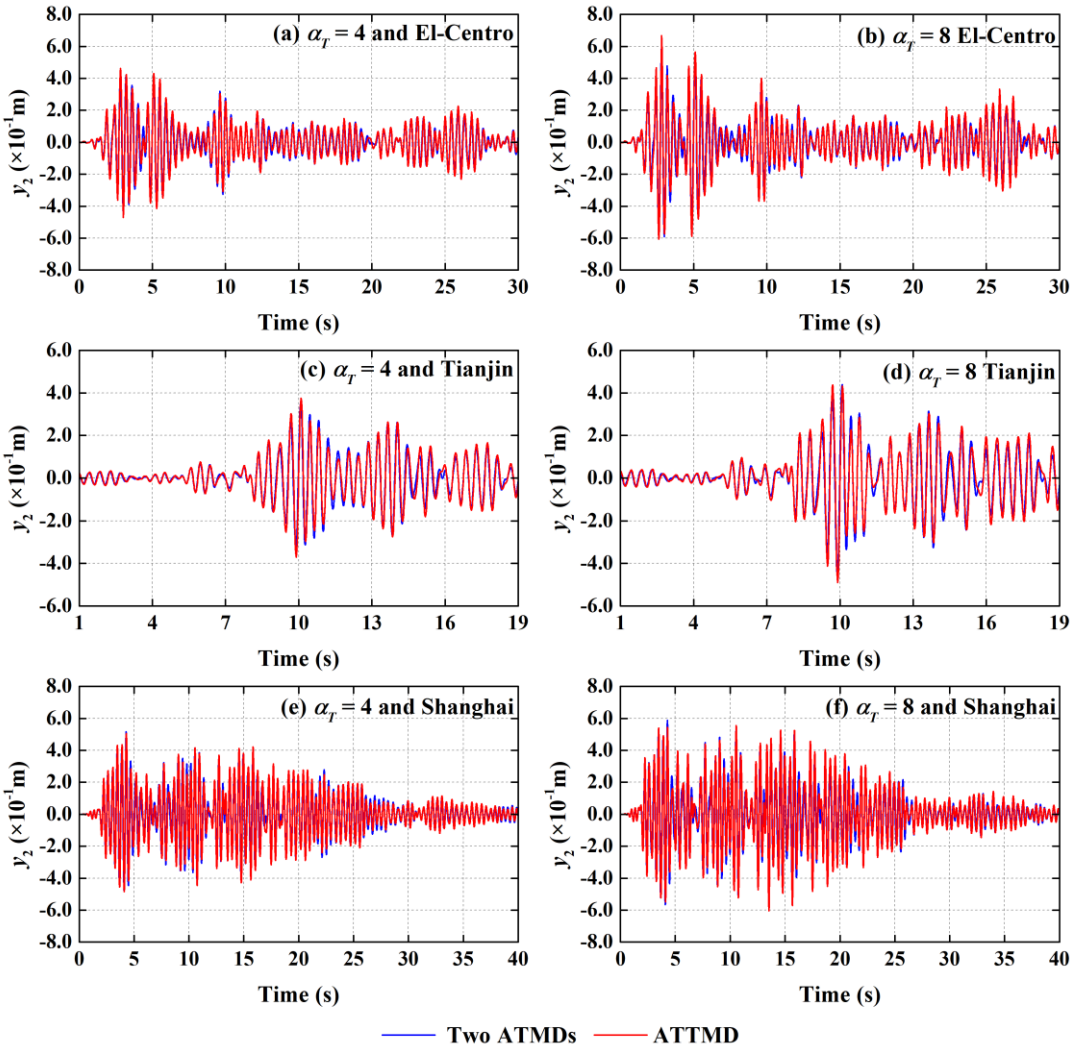

Fig. 20 Time history plots of stroke of the ATMD2 in the optimum ATTMD (taking the optimum linking damping ratio) and optimum Two ATMDs with μ_T=0.01, η=0.25, and γ=1/4 for two normalized acceleration feedback gain factors and three earthquake records: (a) α_T=4 and El-Centro, (b) α_T=8 and El-Centro, (c) α_T=4 and Tianjin, (d) α_T=8 and Tianjin, (e) α_T=4 and Shanghai, and (f) α_T=8 and Shanghai

of three-storey building with and without the optimum ATTMD or optimum Two ATMDs with μ_T=0.01, η=0.25, and γ=1/4 with α_T=4.0 and α_T=8.0 subjected to three earthquakes. For the charts shown in Fig. 18, the following two conclusions can be identified: (1) the ATTMD is capable of reducing the displacement of the three-storey building under earthquakes, and (2) the ATTMD and two ATMDs without the dashpot possesses the nearly identical level of effectiveness.

Fig. 19 shows the time history plots of stroke of the ATMD1 in the optimum ATTMD and optimum Two ATMDs with μ_T=0.01, η=0.25, and γ=1/4 with α_T=4.0 and α_T=8.0 subjected to three earthquakes. As expected, the charts shown in Fig. 19 clearly demonstrate that the stroke of the ATMD1 is much less than that of Two ATMDs.

Fig. 20 presents the time history plots of stroke of the ATMD2 in the optimum ATTMD and optimum Two ATMDs with μ_T=0.01, η=0.25, and γ=1/4 with α_T=4.0 and α_T=8.0 subjected to three earthquakes. Similar to the results in Figs. 15 and 16, under the circumstances of μ_T=0.01, η=0.25, and γ=1/4 with α_T=4.0 and α_T=8.0, at the optimum linking damping ratio the stroke of ATMD2 in the ATTMD is nearly identical to that of two ATMDs without the dashpot.

In order to examine the effect of linking damping ratio in the time domain, Table 7 presents the effectiveness ratios (ER) of investigated ATTMD and Two ATMDs with μ_T=0.01, η=0.25, and γ=1/4 in two cases of the optimum linking damping ratio and ξ_T=0.2 under three earthquakes. In light of Table 7, the following findings can be summarized. Increasing the linking damping ratio, the change is not obvious in the effectiveness ratios (ER) of ATTMD for reduction of the structural displacement. Likewise, the ATTMD keeps the nearly identical effectiveness to Two ATMDs. As regards the stroke of ATTMD, increasing the linking damping ratio can enhance the effectiveness ratio (ER) of ATMD2 but decreases that of ATMD1. Likewise, it is worth pointing out that with the increase of the linking damping ratio, the perturbation in the total stroke (i.e., sum of the stroke of ATMD1 and ATMD2)

Table 7 Effectiveness ratios (ER) of investigated ATTMD and Two ATMDs with μ_T=0.01, η=0.25, and γ=1/4 in two cases of the optimum linking damping ratio (ξ_{Topt}) and ξ_T=0.2 under three earthquakes (%)

		EI-Centro			Tianjin			Shanghai		
α_T	ER_{ysi}	Two ATMDs	ATTMD		Two ATMDs	ATTMD		Two ATMDs	ATTMD	
			ξ_{Topt}	0.2		ξ_{Topt}	0.2		ξ_{Topt}	0.2
4	ER_{ys1}	30.13	**29.29**	31.87	40.58	**42.12**	41.30	39.00	**37.26**	35.22
	ER_{ys2}	28.54	**27.70**	30.42	41.58	**43.17**	42.37	39.00	**37.33**	35.44
	ER_{ys3}	26.61	**25.81**	28.28	41.84	**43.61**	43.01	38.87	**37.25**	35.64
	ER_{y1}		**38.31**	29.15		**33.17**	22.99		**39.97**	29.79
	ER_{y2}		**-6.25**	6.26		**-6.86**	6.53		**2.00**	9.6
8	ER_{ys1}	32.67	**32.25**	32.98	48.82	**48.56**	48.33	40.89	**40.22**	39.12
	ER_{ys2}	29.54	**29.37**	30.17	50.88	**51.47**	50.65	40.82	**40.26**	39.01
	ER_{ys3}	27.43	**27.62**	28.56	51.26	**51.86**	51.37	40.94	**41.68**	39.10
	ER_{y1}		**36.81**	25.69		**35.04**	24.58		**38.84**	27.18
	ER_{y2}		**-8.92**	2.83		**-6.54**	5.96		**-2.85**	6.55

Note: $ER_{yi} = \dfrac{\text{Peak displacement of uncontrolled structure} - \text{Peak displacement of controlled structure}}{\text{Peak displacement of uncontrolled structure}} \times 100\%$, $i = 1, 2, s1, s2, s3$

is very small, thus analogous to the results in the frequency domain.

Thus it can be seen that the findings of the effectiveness and stroke in the time domain are well agreement with the ones in the frequency domain.

5. Conclusions

Employing the derived objective function of the structure installed with the ATTMD and the gradient-based searching technique, the optimum ATTMD is systematically evaluated and thoroughly compared with the optimum two ATMDs, two TMDs, and TTMD in the frequency domain. Subsequent to work in the frequency domain, the real-time Simulink implementation of dynamic analysis of the structure with the ATTMD under three earthquakes is conducted to corroborate the findings of the effectiveness and stroke in the frequency domain. The three earthquakes include two actual El-Centro and Tianjin records and one artificial Shanghai record. In accordance with the extensive numerical results obtained and assessment presented, the main conclusions can be drawn as follows:

(1) Employing the derived closed-form expression of the objective function of the structure-ATTMD system, the gradient-based optimization technique is capable of making precise determination on the ATTMD parameters.

(2) Given a total mass ratio of the ATTMD, such as μ_T=0.01, the appropriate combination of both the mass ratio between ATMD1 and ATMD2 as well as the allocation ratio of their control forces, such as η=0.25 and γ=1/4, can bring about the optimum effectiveness of the ATTMD. Likewise, the ATTMD and two ATMDs without the linking dashpot possesses the nearly identical level of effectiveness, but remarkably higher than that of the TTMD and two TMDs.

(3) The frequency spacing characterizing the robustness of the ATTMD is obviously larger than that of the TTMD and by a long way exceeds those of two ATMDs and two TMDs without the linking dashpot. Likewise, the frequency spacing of the ATTMD is comparable to that of the AMTMD.

(4) The optimum damping ratios of the ATMD1 and ATMD2 are simultaneously equal to zero. That is, neither of them needs dampers. This property manifestly simplifies the composition of the ATTMD, thereby further highlighting its simplicity and practicability for application.

(5) The stroke of the ATMD1 is much less than that of Two ATMDs. At the optimum linking damping ratio the stroke of ATMD2 in the ATTMD is nearly identical to that of two ATMDs without the linking dashpot. Likewise increasing the linking damping ratio can reduce the stroke of ATMD2.

(6) Representative numerical results in the time domain support the findings of the effectiveness and stroke in the frequency domain.

Therefore, the ATTMD with the least number of ATMD units is deemed to be a high robustness control device and doesn't reduce the effectiveness. Likewise, the stroke of the ATTMD is smaller than that of two ATMDs without a linking dashpot. The ATTMD system only needs the linking dashpot, thus embodying its simplicity. Furthermore, the ATTMD may be designed and implemented in accordance with the technical guidelines and engineering practical experiences for the ATMD.

In closing, we present the layout principle of the ATTMD for seismic plan-asymmetric structures to promote its wider practical applications. For one-way plan-asymmetric structures, In order to reduce the structural translational and torsional responses more effectively, the smaller ATMD is installed at the stiff edge which is near to the centre of stiffness (CS), while the larger ATMD is set at the flexible edge which is away from the CS. For two-way plan-asymmetric structures, the same arrangement principle

can be adopted, but two sets of ATTMD are required.

References

Amini, F., Hazaveh, N.K. and Rad, A.A. (2013), "Wavelet PSO-based LQR algorithm for optimal structural control using active tuned mass dampers", *Comput. Aid. Civil Infrastr. Eng.*, **28**(7), 542-557. https://doi.org/10.1111/mice.12017.

Angelis, M.D., Perno, S. and Reggio, A. (2012), "Dynamic response and optimal design of structures with large mass ratio TMD", *Earthq. Eng. Struct. Dyn.*, **41**(1), 41-60. https://doi.org/10.1002/eqe.1117.

Ankireddi, S. and Yang, H.T.Y. (1996), "Simple ATMD control methodology for tall buildings subject to wind loads", *J. Struct. Eng.*, ASCE, **122**(1), 83-91. https://doi.org/10.1061/(ASCE)0733-9445(1996)122:1(83).

Basu, B. and Nagarajaiah, S. (2008), "A wavelet-based time-varying adaptive LQR algorithm for structural control", *Eng. Struct.*, **30**(9) 2470-2477. https://doi.org/10.1016/j.engstruct.2008.01.011.

Bekdaş, G. and Nigdeli, S.M. (2013), "Mass ratio factor for optimum tuned mass damper strategies", *Int. J. Mech. Sci.*, **71**, 68-84. https://doi.org/10.1016/j.ijmecsci.2013.03.014.

Cao, L. and Li, C. (2018), "Enhanced hybrid active tuned mass dampers for structures", *Struct. Control Hlth. Monit.*, **25**(2), e2067. https://doi.org/10.1002/stc.2067.

Cao, L. and Li, C. (2019), "Tuned tandem mass dampers-inerters with broadband high effectiveness for structures under white noise base excitations", *Struct. Control Hlth. Monit.*, **26**(4), e2319. https://doi.org/ 10.1002/stc.2319.

Carpineto, N., Lacarbonara, W. and Vestroni, F. (2014), "Hysteretic tuned mass dampers for structural vibration mitigation", *J. Sound Vib.*, **333**(5), 1302-1318. https://doi.org/10.1016/j.jsv.2013.10.010.

Casalotti, A., Arena, A. and Lacarbonara, W. (2014), "Mitigation of post-flutter oscillations in suspension bridges by hysteretic tuned mass dampers", *Eng. Struct.*, **69**, 62-71. https://doi.org/10.1016/j.engstruct.2014.03.001.

Chang, C.C. and Yang, H.T.Y. (1995), "Control of buildings using active tuned mass dampers", *J. Eng. Mech.*, ASCE, **121**(3), 355-366. https://doi.org/10.1061/(ASCE)0733-9399(1995)121:3(355).

Chang, J.C.H. and Soong, T.T. (1980), "Structural control using active tuned mass damper", *J. Eng. Mech.*, ASCE, **106**(6), 1091-1098.

Chen, G. and Wu, J. (2001), "Optimal placement of multiple tuned mass dampers for seismic structures", *J. Struct. Eng.*, ASCE, **127**(9), 1054-1062. https://doi.org/10.1061/(ASCE)0733-9445(2001)127:9(1054).

Chey, M.H., Chase, J.G., Mander, J.B. and Carr, A.J. (2010), "Semi-active tuned mass damper building systems: Design", *Earthq. Eng. Struct. Dyn.*, **39**(2), 119-139. https://doi.org/10.1002/eqe.934.

Chung, L.L., Lai, Y.A., Yang, C.S.W., Lien, K.H. and Wu, L.Y. (2013), "Semi-active tuned mass dampers with phase control", *J. Sound Vib.*, **332**(15), 3610-3625. https://doi.org/10.1016/j.jsv.2013.02.008.

Chung, L.L., Wu, L.Y., Walter Yang, C.S.W., Lien, K.H., Lin, M.C. and Huang, H.H. (2013), "Optimal design formulas for viscous tuned mass dampers in wind-excited structures", *Struct. Control Hlth. Monit.*, **20**(3), 320-336. https://doi.org/10.1002/stc.496.

Collins, R., Basu, B. and Broderick, B. (2006), "Control strategy using bang-bang and minimax principle for FRF with ATMDs", *Eng. Struct.*, **28**(3), 349-356. https://doi.org/10.1016/j.engstruct.2005.08.012.

Daniel, Y., Lavan, O. and Levy, R. (2012), "Multiple-tuned mass dampers for multimodal control of pedestrian bridges", *J. Struct. Eng.*, ASCE, **138**(9), 1173-1178. https://doi.org/10.1061/(ASCE)ST.1943-541X.0000527.

Dinh, V.N. and Basu, B. (2015), "Passive control of floating offshore wind turbine nacelle and spar vibrations by multiple tuned mass dampers", *Struct. Control Hlth. Monit.*, **22**(1), 152-176. https://doi.org/10.1002/stc.1666.

Domaneschi, M., Martinelli, L. and Po, E. (2015), "Control of wind buffeting vibrations in a suspension bridge by TMD: Hybridization and robustness issues", *Comput. Struct.*, **155**, 3-17. https://doi.org/10.1016/j.compstruc.2015.02.031.

Erduran, E. (2012), "Evaluation of Rayleigh damping and its influence on engineering demand parameter estimates", *Earthq. Eng. Struct. Dyn.*, **41**(14), 1905-1919. https://doi.org/10.1002/eqe.2164.

Fitzgerald, B. and Basu, B. (2014), "Cable connected active tuned mass dampers for control of in-plane vibrations of wind turbine blades", *J. Sound Vib.*, **333**(23), 5980-6004. https://doi.org/10.1002/stc.1524.

Fu, T.S. and Johnson, E.A. (2011), "Distributed mass damper system for integrating structural and environmental controls in buildings", *J. Eng. Mech.*, ASCE, **137**(3), 205-213. https://doi.org/10.1061/(ASCE)EM.1943-7889.0000211.

Gu, M., Xiang, H.F. and Chen, A.R. (1994), "A practical method of TMD for suppressing wind-induced vertical buffeting of long-span cable-stayed bridges and its application", *J. Wind Eng. Ind. Aerodyn.*, **51**(2), 203-213. https://doi.org/10.1016/0167-6105(94)90004-3.

Guclu, R. and Yazici, H. (2008), "Vibration control of a structure with ATMD against earthquake using fuzzy logic controllers", *J. Sound Vib.*, **318**(1-2), 36-49. https://doi.org/10.1016/j.jsv.2008.03.058.

Jangid, R.S. (1995), "Dynamic characteristics of structures with multiple tuned mass dampers", *Struct. Eng. Mech.*, **3**(5), 497-509. https://doi.org/10.12989/sem.1995.3.5.497.

Jangid, R.S. (1999), "Optimum multiple tuned mass dampers for base-excited undamped system", *Earthq. Eng. Struct. Dyn.*, **28**(9), 1041-1049. https://doi.org/10.1002/(SICI)1096-9845(199909)28:9.

Jokic, M., Stegic, M. and Butkovic, M. (2011), "Reduced-order multiple tuned mass damper optimization: A bounded real lemma for descriptor systems approach", *J. Sound Vib.*, **330**(22), 5259-5268. https://doi.org/10.1016/j.jsv.2011.06.005.

Kaiming, B. and Hong, H. (2016), "Using pipe-in-pipe systems for subsea pipeline vibration control", *Eng. Struct.*, **109**, 75-84. https://doi.org/10.1016/j.engstruct.2015.11.018.

Kareem, A. and Kline, S. (1995), "Performance of multiple mass dampers under random loading", *J. Struct. Eng.*, ASCE, **121**(2), 348-361. https://doi.org/10.1061/(ASCE)0733-9445(1995)121:2(348).

Kaveh, A., Mohammadi, Khademhosseini, S., Keyhani, O.A. and Kalatjari, V.R. (2015), "Optimum parameters of tuned mass dampers for seismic applications using charged system search", *Iran. J. Sci. Tech., Trans. Civil Eng.*, **39**(C1), 21-40.

Kaveh, A., Pirgholizadeh, S. and Khademhosseini, O. (2015), "Semi-active tuned mass damper performance with optimized fuzzy controller using CSS algorithm", *Asian J. Civil Eng.*, **16**(5), 587-606.

Lavan, O. (2017), "Multi-objective optimal design of tuned mass dampers", *Struct. Control Hlth. Monit.*, **24**(11), e2008. https://doi.org/10.1002/stc.2008.

Leung, A.Y.T. and Zhang, H. (2009), "Particle swarm optimization of tuned mass dampers", *Eng. Struc.*, **31**, 715-728. https://doi.org/10.1016/j.engstruct.2008.11.017.

Li, C and Cao, L. (2019). "High performance active tuned mass damper inerter for structures under the ground acceleration",

Earthq. Struct., **16**(2), 149-163. https://doi.org/10.12989/eas.2019.16.2.149.

Li, C. (2000), "Performance of multiple tuned mass dampers for attenuating undesirable oscillations of structures under the ground acceleration", *Earthq. Eng. Struct. Dyn.*, **29**(9), 1405-1421. https://doi.org/10.1002/1096-9845(200009)29:9.

Li, C. and Cao, B. (2015), "Hybrid active tuned mass dampers for structures under the ground acceleration", *Struct. Control Hlth. Monit.*, **22**(4), 757-773. https://doi.org/10.1002/stc.1716.

Li, C. and Liu, Y. (2002), "Active multiple tuned mass dampers for structures under the ground acceleration", *Earthq. Eng. Struct. Dyn.*, **31**(5), 1041-1052. https://doi.org/10.1002/eqe.136.

Li, C. and Liu, Y. (2002), "Further characteristics for multiple tuned mass dampers", *J. Struct. Eng.*, ASCE, **128**(10), 1362-1365. https://doi.org/10.1061/(ASCE)0733-9445(2002)128:10(1362).

Li, C. and Liu, Y. (2003), "Optimum multiple tuned mass dampers for structures under ground acceleration based on the uniform distribution of system parameters", *Earthq. Eng. Struct. Dyn.*, **32**(5), 671-690. https://doi.org/10.1002/eqe.239.

Li, C. and Qu, W. (2006), "Optimum properties of multiple tuned mass dampers for reduction of translational and torsional response of structures subject to ground acceleration", *Eng. Struct.*, **28**(4), 472-494. https://doi.org/10.1016/j.engstruct.2005.09.003.

Li, C. and Zhu, B. (2006), "Estimating double tuned mass dampers for structures under the ground acceleration using a novel optimum criterion", *J. Sound Vib.*, **298**(1-2), 280-297. https://doi.org/10.1016/j.jsv.2006.05.018.

Li, C., Li, J. and Qu, Y. (2010), "An optimum design methodology of active tuned mass damper for asymmetric structures", *Mech. Syst. Signal Pr.*, **24**(3), 746-765. https://doi.org/10.1016/j.ymssp.2009.09.011.

Li, C., Liu, Y. and Wang, Z. (2003), "Active multiple tuned mass dampers: a new control strategy", *J. Struct. Eng.*, ASCE, **129**(7), 972-977. https://doi.org/10.1061/(ASCE)0733-9445(2003)129:7(972).

Li, H.N., Zhang, P., Song, G., Patil, D. and Mo, Y. (2015), "Robustness study of the pounding tuned mass damper for vibration control of subsea jumpers", *Smart Mater. Struct.*, **24**(9), 095001.

Lin, C.C., Lu, L.Y., Lin, G.L. and Yang, T.W. (2010), "Vibration control of seismic structures using semi-active friction multiple tuned mass dampers", *Eng. Struct.*, **32**(10), 3404-3417. https://doi.org/10.1016/j.engstruct.2010.07.014.

Lin, C.C., Wang, J.F., Lien, C.H., Chiang, H.W. and Lin, C.S. (2010), "Optimum design and experimental study of multiple tuned mass dampers with limited stroke", *Earthq. Eng. Struct. Dyn.*, **39**(14), 1631-1651. https://doi.org/10.1002/eqe.1008.

Lin, G.L., Lin, C.C., Chen, B.C. and Soong, T.T. (2015), "Vibration control performance of tuned mass dampers with resettable variable stiffness", *Eng. Struct.*, **83**, 187-197. https://doi.org/10.1016/j.engstruct.2014.10.041.

Lin, G.L., Lin, C.C., Lu, L.Y. and Ho, Y.B. (2012), "Experimental verification of seismic vibration control using a semi-active friction tuned mass damper", *Earthq. Eng. Struct. Dyn.*, **41**(4), 813-830. https://doi.org/10.1002/eqe.1162.

Lu, X. and Chen, J. (2011), "Mitigation of wind-induced response of Shanghai Center Tower by tuned mass damper", *Struct. Des. Tall Spec. Build.*, **20**(4), 435-452. https://doi.org/10.1002/tal.659.

Lu, X. and Chen, J. (2011), "Parameter optimization and structural design of tuned mass damper for Shanghai center tower", *Struct Des. Tall Spec Build.*, **20**(4), 453-471. https://doi.org/10.1002/tal.649.

Lu, X., Zhang, Q., Weng, D., Zhou, Z., Wang, S., Mahin, S.A., Ding, S. and Qian, F. (2017), "Improving performance of a super tall building using a new eddy-current tuned mass damper", *Struct. Control Hlth. Monit.*, **24**(3), e1882. https//doi: 10.1002/stc.1882.

Matta, E. (2013), "Effectiveness of tuned mass dampers against ground motion pulses", *J. Struct. Eng.*, ASCE, **139**(2), 188-198. https://doi.org/10.1061/(ASCE)ST.1943-541X.0000629.

Mohebbi, M., Shakeri, K., Ghanbarpour, Y. and Majzoub, H. (2013), "Designing optimal multiple tuned mass dampers using genetic algorithms (GAs) for mitigating the seismic response of structures", *J. Vib. Control*, **19**(4), 605-625. https://doi.org/10.1177/1077546311434520.

Nagarajaiah, S. (2009), "Adaptive passive, semi-active, smart tuned mass dampers: identification and control using empirical mode decomposition, Hilbert transform, and short-term Fourier transform", *Struct. Control Hlth. Monit.*, 1**6**(7-8), 800-841. https://doi.org/10.1002/stc.349.

Nagarajaiah, S. and Sonmez, E. (2007), "Structures with semi-active variable stiffness single/ multiple tuned mass dampers", *J. Struct. Eng.*, ASCE, **133**(1), 67-77. https://doi.org/10.1061/(ASCE)0733-9445(2007)133:1(67).

Nagarajaiah, S. and Varadarajan, N. (2005), "Short time Fourier transform algorithm for wind response control of buildings with variable stiffness TMD", *Eng. Struct.*, **27**(3), 431-441. https://doi.org/10.1016/j.engstruct.2004.10.015.

Nagashima, I. (2001), "Optimal displacement feedback control law for active tuned mass damper", *Earthq. Eng. Struct. Dyn.*, **30**(8), 1221-1242. https://doi.org/10.1002/eqe.60.

Nishitani, A. and Inoue, Y. (2001), "Overview of the application of active/semi-active control to building structures in Japan", *Earthq. Eng. Struct. Dyn.*, **30**(11), 1565-1574. https://doi.org/10.1002/eqe.81.

Ok, S.Y., Song, J. and Park, K.S. (2009), "Development of optimal design formula for bi-tuned mass dampers using multi-objective optimization", *J. Sound Vib.*, **322**(1-2), 60-77. https://doi.org/10.1016/j.jsv.2008.11.023.

Reggio, A. and Angelis, M.D. (2015), "Optimal energy-based seismic design of non-conventional Tuned Mass Damper (TMD) implemented via inter-story isolation", *Earthq. Eng. Struct. Dyn.*, **44**(10), 1623-1642. https://doi.org/10.1002/eqe.2548.

Shu, Z., Li, S., Zhang, J. and He, M. (2017), "Optimum seismic design of a power plant building with pendulum tuned mass damper system by its heavy suspended buckets", *Eng. Struct.*, **136**, 114-132. https://doi.org/10.1016/j.engstruct.2017.01.010.

Si, Y., Karimi, H.R. and Gao, H. (2014), "Modelling and optimization of a passive structural control design for a spar-type floating wind turbine", *Eng. Struct.*, **69**, 168-182. https://doi.org/10.1016/j.engstruct.2014.03.011.

Song, G., Zhang, P., Li, L., Singla, M., Patil, D., Li, H.N. and Mo, Y. (2016), "Vibration control of a pipeline structure using pounding tuned mass damper", *J. Eng. Mech.*, ASCE, **142**(6), 04016031. https://doi.org/10.1061/(ASCE)EM.1943-7889.0001078.

Spanos, P.T.D. (1983), "Spectral moments calculation of linear system output", *J. Appl. Mech.*, ASME, **50**(4), 901-903. https://doi.org/10.1115/1.3167169.

Spencer, B. and Nagarajaiah, S. (2003), "State of the art of structural control", *J. Struct. Eng.*, ASCE, **129**(7), 845-856. https://doi.org/10.1061/(ASCE)0733-9445(2003)129:7(845).

Stăncioiu, D. and Ouyang, H. (2012), "Structural modification formula and iterative design method using multiple tuned mass dampers for structures subjected to moving loads", *Mech. Syst. Signal Pr.*, **28**, 542-560. https://doi.org/10.1016/j.ymssp.2011.11.009.

Stewart, G.M. and Lackner, M.A. (2014), "The impact of passive tuned mass dampers and wind-wave misalignment on offshore wind turbine loads", *Eng. Struct.*, **73**, 54-61. https://doi.org/10.1016/j.engstruct.2014.04.045.

Sun, C. (2018), "Semi-active control of monopile offshore wind turbines under multi-hazards", *Mech. Syst. Signal Pr.*, **99**, 285-305. https://doi.org/10.1016/j.ymssp.2017.06.016.

Sun, C. and Nagarajaiah, S. (2014), "Study on semi-active tuned mass damper with variable damping and stiffness under seismic excitations", *Struct. Control Hlth. Monit.*, **21**(6), 890-906. https://doi.org/10.1002/stc.1620.

Venanzi, I., Ubertini, F. and Materazzi, A.L. (2013), "Optimal design of an array of active tuned mass dampers for wind-exposed high-rise buildings", *Struct. Control Hlth. Monit.*, **20**(6), 903-917. https://doi.org/10.1002/stc.1502.

Weber, F. (2014), "Semi-active vibration absorber based on real-time controlled MR damper", *Mech. Syst. Signal Pr.*, **46**(2-3), 272-288. https://doi.org/10.1016/j.ymssp.2014.01.017.

Weber, F., Boston, C. and Maslanka, M. (2011), "An adaptive tuned mass damper based on the emulation of positive and negative stiffness with an MR damper", *Smart Mater. Struct.*, **20**(1), 015012.

Xu, K. and Igusa, T. (1992), "Dynamic characteristics of multiple substructures with closely spaced frequencies", *Earthq. Eng. Struct. Dyn.*, **21**(12), 1059-1070. https://doi.org/10.1002/eqe.4290211203

Yan, N., Wang, C.M. and Balendra, T. (1999), "Optimum damper characteristics of ATMD for buildings under wind loads", *J. Struct. Eng.*, ASCE, **125**(12), 1376-1383. https://doi.org/10.1061/(ASCE)0733-9445(1999)125:12(1376).

Yang, Y. and Li, C. (2017), "Performance of tuned tandem mass dampers for structures under the ground acceleration", *Struct, Control Hlth. Monit.*, **24**(10), e1974, https://doi.org/10.1002/stc.1974.

Zhang, P., Song, G., Li, H.N. and Lin, Y.X. (2013), "Seismic control of power transmission tower using pounding TMD", *J. Eng. Mech.*, ASCE, **139**(10), 1395-1406. https://doi.org/10.1061/(ASCE)EM.1943-7889.0000576.

Zuo, L. and Nayfeh, S. (2005), "Optimization of the individual stiffness and damping parameters in multiple-tuned-mass-damper systems", *J. Vib. Acoust.*, ASME, **127**(1), 77-83. https://doi.org/10.1115/1.1855929.

AT